Late Quaternary activity and seismic potential of the Santa Monica fault system, Los Angeles, California

James F. Dolan*
Department of Earth Sciences, University of Southern California, Los Angeles, California 90089-0740, USA

Kerry Sieh
Seismological Laboratory, California Institute of Technology 252-21, Pasadena, California 91125, USA

Thomas K. Rockwell
Department of Geological Sciences, San Diego State University, San Diego, California 92182, USA

ABSTRACT

The Santa Monica fault is a 40-km-long, oblique left-lateral reverse fault that extends through the densely urbanized northwestern Los Angeles, California, area and offshore parallel to the Malibu coast. The fault exhibits near-surface strain partitioning in paleoseismologic trenches, and has undergone at least six surface ruptures during the past ~50 k.y. Although events may be missing from the older part of the record, and the ages of older events are based on poorly constrained soil age estimates, at least two and probably three events occurred after the well-dated burial of a prominent paleosol ca. 16–17 ka. The resulting ~7–8 k.y. latest Pleistocene–Holocene average recurrence interval for events large enough to cause surface rupture is much longer than the ≤1.9–3.3 k.y. maximum interval we calculate for hypothetical M_w 6.9–7.0 earthquakes generated by rupture of the entire Santa Monica fault. The pronounced disparity between the measured and calculated average recurrence intervals suggests that the Santa Monica fault undergoes infrequent, and therefore probably very large, earthquakes ($M_w \geq 7.0$). If such large earthquakes have occurred, we speculate that they may have been generated by simultaneous rupture of the Santa Monica fault with other faults in the Transverse Ranges Southern Boundary fault system, such as the Hollywood or Anacapa-Dume faults. The most recent definite Santa Monica fault surface rupture occurred between ca. 10 and 17 ka, although a more recent event probably occurred between ca. 1 and 3 ka.

Keywords: earthquakes, faulting, geomorphology, paleoseismology, seismic risk, seismic zoning.

INTRODUCTION

During the past decade ideas about the seismic hazards facing urban Los Angeles have undergone dramatic revision and refinement. Earlier earthquake scenarios for the metropolitan region focused primarily on the effects of a great ($M_w \sim 8$) earthquake generated by the San Andreas fault, which is located more than 50 km northeast of downtown Los Angeles (Fig. 1). Widespread attention did not begin to focus on the potential hazards posed by faults directly beneath the metropolitan area until the mid-1980s (e.g., Wesnousky, 1986; Toppozada, 1988). The 1987 M_w 6.0 Whittier Narrows earthquake, and more recently the 1994 M_w 6.7 Northridge earthquake, clearly demonstrated the seismic hazards associated with these urban faults. Consequently, seismic hazard assessments of the past several years focus on the possibility of large urban earthquakes, as well as the occurrence of major earthquakes produced by the San Andreas fault (e.g., WGCEP, 1995).

Because of their proximity to metropolitan Los Angeles, large earthquakes (M_w 7.0–7.5) generated by the urban faults could cause at least as much damage as a much larger earthquake occurring on the more distant San Andreas fault, and possibly more (WGCEP, 1995; Dolan et al., 1995; Heaton et al., 1995). At least two such large earthquakes have occurred during historic time in southern California on faults similar to those that underlie the metropolitan region: the December 21, 1812, M ~ 7.1 Santa Barbara Channel earthquake (Toppozada et al., 1981) and the July 21, 1952, $M_w \sim 7.5$ Kern County event (Hanks et al., 1975; Stein and Thatcher, 1981; Ellsworth, 1990). Fortunately, neither of these earthquakes resulted in widespread damage or major loss of life, because both regions were relatively sparsely populated at the time of the earthquakes.

Despite a heightened awareness of the potential for destructive earthquakes from faults beneath metropolitan Los Angeles, as well as numerous recent studies that have illuminated the active tectonics of the region (e.g., Hauksson, 1990; Wright, 1991; Dolan et al., 1995; Shaw and Suppe, 1996; Schneider et al., 1996; Walls et al., 1998; Shaw and Shearer, 1999; Argus et al., 1999; Tsutsumi et al., 2000), relatively little information exists about the earthquake histories and recent kinematics of many faults in the metropolitan region. Specifically, we have only sparse data concerning recurrence intervals, dates, and sizes of past events, slip rates, and kinematics of fault movement for many structures. Furthermore, we do not know the exact nature and location of the surficial expressions of many of these faults. Knowledge of these fault parameters is an essential part of the foundation for construction of seismic hazard models for southern California.

In this paper we discuss our results from the Santa Monica fault, which extends 40 km through the densely urbanized northwestern

*E-mail: dolan@earth.usc.edu.

GSA Bulletin; October 2000; v. 112; no. 10; p. 1559–1581; 11 figures; 1 table.

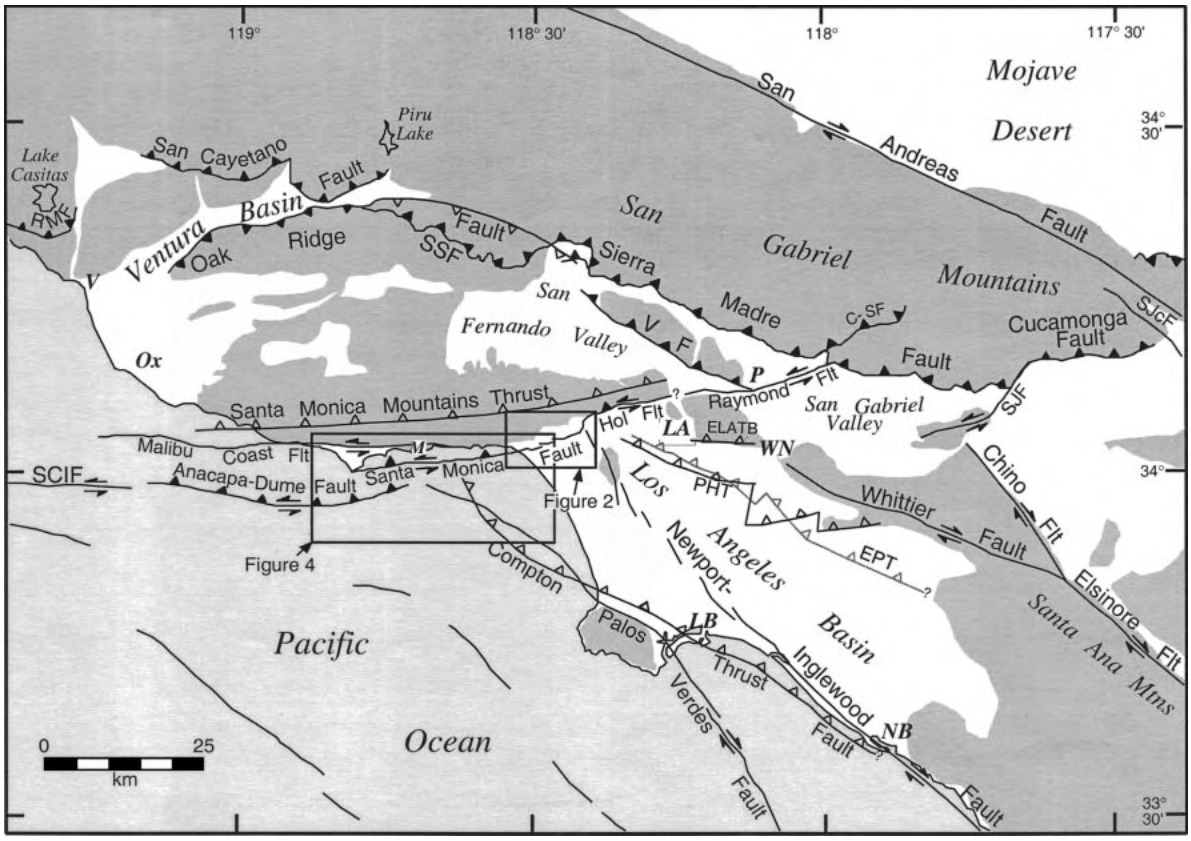

1. Regional neotectonic map for metropolitan southern California showing major active faults. The Santa Monica fault is a 40-km-long active fault within the 215-km-long Transverse Ranges Southern Boundary fault system (TRSBFS), which encompasses the Raymond, Hollywood, Santa Monica, Malibu Coast, Anacapa-Dume, Santa Cruz Island, and Santa Rosa Island faults as well as several blind thrust faults. Fault locations are from Ziony and Jones (1989), Vedder et al. (1986), Dolan and Sieh (1992), Sorlien (1994), and Dolan et al. (1997). Santa Rosa Island fault is off figure to west. Closed teeth denote reverse fault surface trace; open teeth on dashed lines show upper edge of blind thrust fault ramps. Strike-slip fault surface traces are shown by double arrows. C-SF—Clamshell-Sawpit fault; ELATB—East Los Angeles blind thrust system; EPT—Elysian park blind thrust fault; Hol Flt—Hollywood fault; PHT—Puente Hills blind thrust fault; RMF—Red Mountain fault; SCIF—Santa Cruz Island fault; SSF—Santa Susana fault; SJcF—San Jacinto fault; SJF—San Jose fault; VF—Verdugo fault; LA—Los Angeles; LB—Long Beach; NB—Newport Beach; Ox—Oxnard; P—Pasadena; V—Ventura; WN—Whittier Narrows. Point Dume is at west end of Santa Monica fault. Downtown Hollywood is centered between Hol and Flt in figure. Dark shading shows Santa Monica Mountains.

Los Angeles region and offshore along the Malibu coast. We first describe the results of our geomorphologic and paleoseismologic studies of the fault and then discuss the implications of these results for seismic hazard assessment in the metropolitan Los Angeles region. We conclude by using estimates of slip rate and fault-plane area to assess the likely size and frequency of future earthquakes on the Santa Monica fault.

REGIONAL GEOLOGY

The Santa Monica fault is part of a system of west-trending reverse, oblique-slip, and left-lateral strike-slip faults that extends for >200 km along the southern edge of the Transverse Ranges, an east-west belt of ranges that has developed in response to north-south compression that began sometime between ca. 2.5 and 5 Ma (Fig. 1) (e.g., Barbat, 1958; Davis et al., 1989; Wright, 1991; Shaw and Suppe, 1996; Schneider et al., 1996; Shaw and Shearer, 1999; Tsutsumi et al., 2000). We refer to these faults collectively as the Transverse Ranges Southern Boundary fault system. Within this fault system, left-lateral and oblique-reverse, left-lateral motion on a subsystem comprising the Raymond, Hollywood, Santa Monica, Anacapa-Dume, Santa Cruz Island, and Santa Rosa Island faults accommodates relative westward motion of the Transverse Ranges block (Stierman and Ellsworth, 1976; Patterson, 1979; Jones et al., 1990; Pinter and Sorlien, 1991; Dolan and Sieh, 1992; Colson et al., 1995; Pinter et al., 1995; Dolan et al., 1995, 1997, 2000; Weaver and Dolan, 2000). Paleomagnetic studies of upper Pliocene strata (1–3 Ma) reveal 20° of clockwise rotation of parts of the western Transverse Ranges block (Liddicoat, 1992), suggesting that left-lateral motion is accompanied by active clockwise rotation of the western Transverse Ranges.

The basic structure of the northwestern Los Angeles basin has been revealed through a combination of extensive oil exploration and regional mapping studies over the past century (see Wright, 1991, for a comprehensive review). These studies show that the Santa Monica fault extends east-west along the southern edge of the Santa Monica Mountains, the southernmost of the Transverse Ranges (Figs. 1 and 2). The range has an asymmetric, anticlinal structure that has been interpreted as a

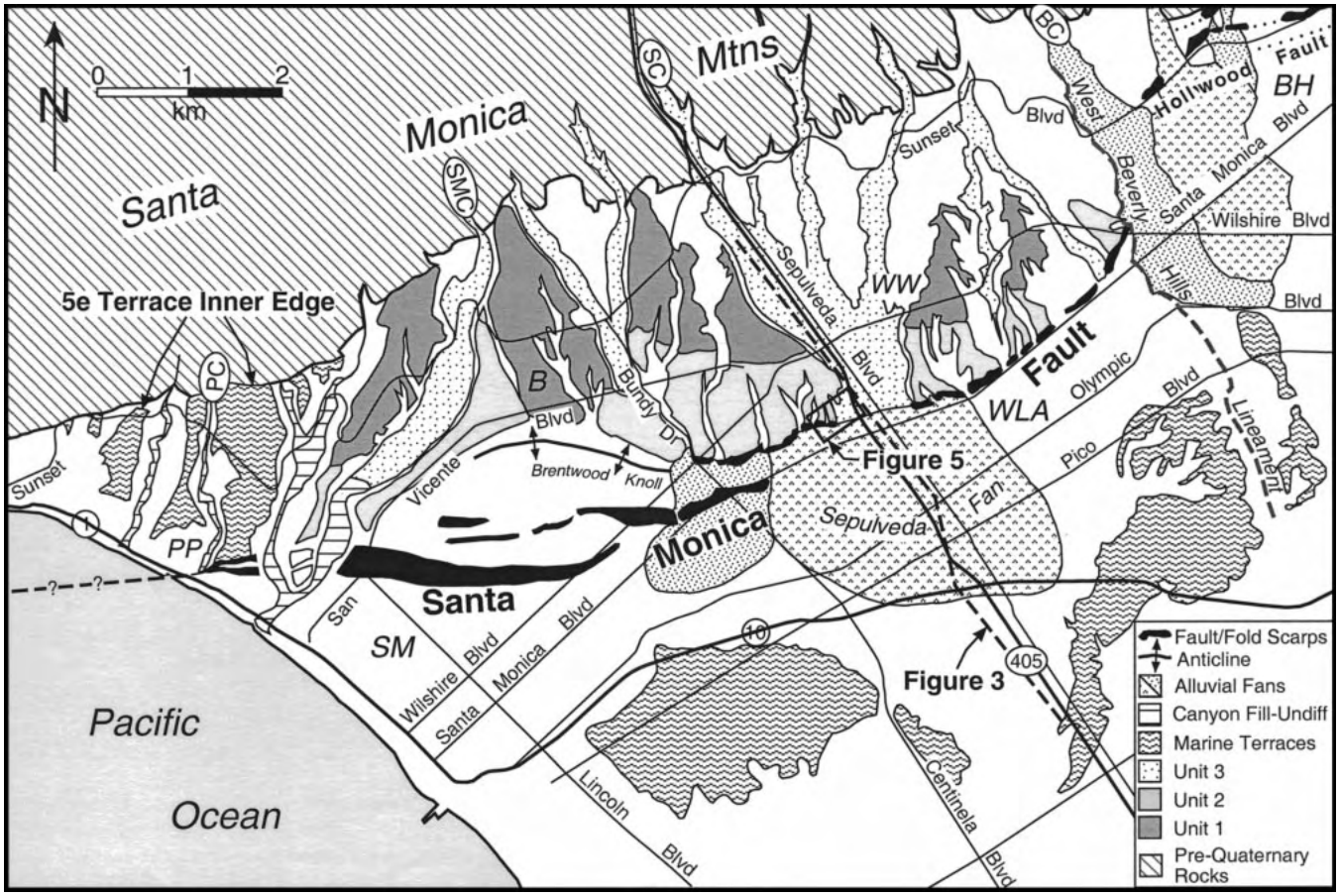

Figure 2. Tectonic geomorphologic map of the Santa Monica fault zone and environs based on interpretation of 1926 vintage U.S. Geological Survey 6 ft topographic maps (Sawtelle, Topanga Canyon, and Hollywood quadrangles) and field mapping. Note location of trench site just west of Freeway I-405. B—Brentwood; BH—Beverly Hills; PC—Potrero Canyon; PP—Pacific Palisades; SM—Santa Monica; WLA—west Los Angeles; WW—Westwood.

fault-propagation fold above a gently north dipping blind thrust fault (Davis et al., 1989; Davis and Namson, 1994). Interpretations of oil-well and seismic reflection data reveal that the north-dipping Santa Monica fault zone comprises two major strands that merge at a depth of ~2 km (Fig. 3) (Wright, 1991; Tsutsumi et al., 2000). The structurally lower, more southerly strand exhibits >3 km of north-side-up reverse separation of middle Miocene (lower Mohnian) strata (Wright, 1991; Tsutsumi et al., 2000). This southern strand is a structurally inverted Miocene normal fault that was active as a reverse fault between latest Miocene and latest Pliocene time (ca. 1.5−5 Ma); Quaternary strata are not deformed by this strand (Wright, 1991; Tsutsumi et al., 2000). The northern strand, which forms the focus of this study, is a moderately steep, north-dipping fault that projects to the surface at a prominent south-facing scarp (discussed in detail in the following). The fault dips moderately to steeply north in the upper 2 km, and rolls over into a shallower dip near the surface (Fig. 3) (Dolan and Pratt, 1997; Pratt et al., 1998). Tsutsumi et al. (2000) show a dip of ~55° at 2 km depth, but comparison with data in Dolan and Pratt (1997) and Pratt et al. (1998) indicates that the fault must dip ~70° north between 200 m and 2 km depth. Reverse separation of middle Miocene (lower Mohnian) strata is ~200 m (Tsutsumi et al., 2000), whereas thrust separation of the base of Pleistocene alluvial strata (including fault slip and near-field drag folding) is ~180 m (Dolan and Pratt, 1997; Pratt et al., 1998). This comparison indicates that almost all motion on the northern strand has occurred during Pleistocene and Holocene time. These observations confirm that Quaternary activity on the Santa Monica fault is concentrated along the northern strand.

GEOMORPHOLOGIC RESULTS

The surface trace of the onshore part of the Santa Monica fault traverses alluvium over most of its length. Consequently, because previous workers made limited use of geomorphologic mapping, the exact location of the fault was known at only few sites (Hoots, 1931; Johnson, 1932; Hill, 1979; Hill et al., 1979; Crook et al., 1983; McGill, 1989; Crook and Proctor, 1992). Earlier maps of the fault were based primarily on interpolation of the trace between the few known localities and on updip and lateral extrapolation of subsurface discontinuities observed in oil and water wells (e.g., Hill et al., 1979; Crook et al., 1983).

In spite of dense urbanization, however, the geomorphologic signature of recent surface faulting along the Santa Monica fault is surprisingly well preserved. Fault and fold scarps are clearly visible on high-quality topographic maps of the alluvial plain between Beverly Hills and the coast. Although this part of the Los Angeles region is completely urbanized, construction occurred primarily during the 1920s, before the widespread use of mechanized grading equipment. Rather than leveling

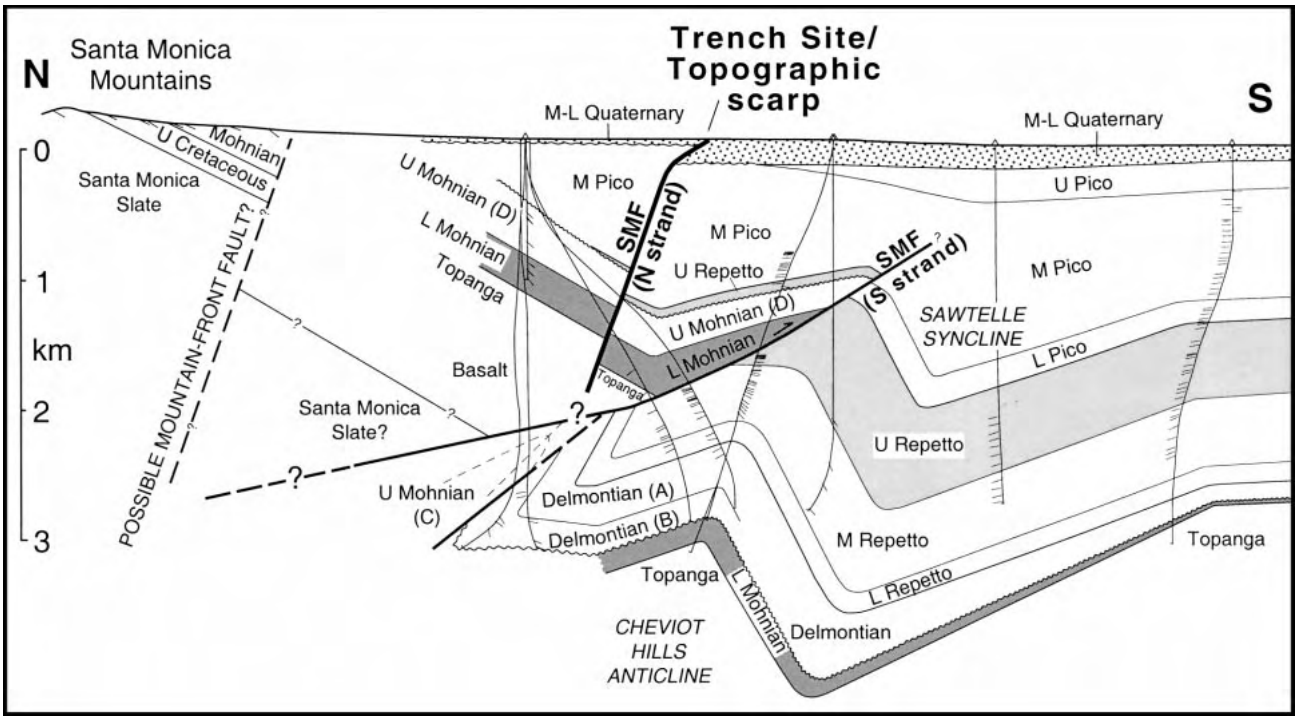

Figure 3. North-northwest−trending cross section showing active (northern) and inactive (southern) strands of the Santa Monica fault zone and associated structures in the vicinity of our trench site (location shown in Fig. 2). Modified from Tsutsumi et al. (2000) on the basis of high-resolution seismic reflection profiles across the upper 200 m of the active strand of the fault (Dolan and Pratt, 1997; Pratt et al., 1998). Data from Dolan and Pratt (1997) and Pratt et al. (1998) are shown projected 400 m eastward onto main cross- section line. Thin, subvertical lines are petroleum wells showing dip-meter data (Tsutsumi et al., 2000). L—lower; M—middle; U—upper; SMF—Santa Monica fault; S strand—southern strand; N strand—northern strand.

building plots, as would be done now, the builders simply draped the city across the existing landscape with minimal cutting and filling.

Our analysis of tectonic landforms along the fault was greatly facilitated by a series of 1:24 000 topographic maps constructed for Los Angeles County by the U.S. Geological Survey during the mid-1920s. These highly detailed maps have a 5 ft (1.5 m) contour interval on relatively gentle terrain, and a 25 ft (7.6 m) interval in mountainous areas. Once we had located the most likely fault-related landforms using the topographic maps, we field checked all suspected features. Our field analyses allowed us to distinguish many features related to grading. These geomorphologic observations, in conjunction with the geotechnical data presented herein, enabled us to construct the first detailed map of the most recently active surface trace of the Santa Monica fault zone (Fig. 2).

Geomorphology of the Northwestern Los Angeles Basin

The broad alluvial plain that extends southward from the Santa Monica Mountains exhibits two geomorphologically distinct provinces. To the east, in Beverly Hills and Hollywood, a steep alluvial front characterized by numerous small, active alluvial fans merges southward into a very gently south sloping alluvial apron. The Hollywood fault, the main active surficial fault in that region, crops out along the base of the mountains (Dolan et al., 1997) (Fig. 1). In contrast, in Santa Monica, Westwood, and west Los Angeles, the area south of the mountain front is characterized by deeply dissected, segmented old alluvial fans and two irregularly shaped flights of marine terraces (Fig. 2). The N20W-trending west Beverly Hills lineament, which is defined by discontinuous east-facing scarps, divides the two geomorphic provinces (Dolan and Sieh, 1992). The lineament may represent an east-dipping normal fault associated with extension along the left step between the Hollywood and Santa Monica faults (Dolan et al., 1997). Alternatively, the west Beverly Hills lineament may be the northernmost of the en echelon, left-stepping, right-lateral strike-slip faults that characterize the Newport-Inglewood structural zone (Dolan and Sieh, 1992), or the surficial manifestation of a northern extension of the gently east-dipping Compton blind thrust fault, identified to the south by Shaw and Suppe (1996).

West of the west Beverly Hills lineament cut-and-fill relationships and changes in surface slopes reveal three sets of major old alluvial surfaces, herein referred to as surfaces 1 (oldest), 2, and 3 (youngest). Surface 1 dips 2.0°–2.5°S and has been deeply incised; only scattered, poorly preserved remnants are preserved in the east. To the west, however, well-preserved segments of this set of old fan surfaces occur near Santa Monica Canyon. Surface 2 remnants are distinguished from the surface 1 fan segments by their shallower dip (1.5°S) and a distinct but irregular break in slope ~2.0–2.5 km south of the mountain front. Surface 2 is best preserved to the east of Santa Monica Canyon, where it is incised into surface 1 by as much as 20 m. There the development of surface 2 clearly postdates the formation of surface 1. West of Sepulveda Canyon surfaces 1 and 2 merge southward with a gently south-dipping alluvial apron. This apron may represent the southward continuation of unit 2, but uplift of a young anticline in this area (Brentwood Knoll, dis-

cussed herein) precludes direct correlation on the basis of topographic relationships. A very gently sloping alluvial apron (unpatterned area in Fig. 2) occurs to the south of older alluvial surfaces 1 and 2. The two older surfaces (1 and 2) are deeply incised by the youngest major alluvial surface, surface 3, which constitutes the gently dipping (~1°S) channel fill of the most recently incised canyons draining the Santa Monica Mountains. Sepulveda and Santa Monica Canyons represent the largest of these drainages. Maximum relief between surfaces 1 and 3 in Santa Monica Canyon is ~42 m. Coastal erosion of all three of these alluvial units has produced spectacular 30–65-m-high cliffs along the Santa Monica–Pacific Palisades shoreline. Near the mouth of Santa Monica Canyon, surface 3 is incised by several smaller terraces.

A wide marine terrace is exposed west of Santa Monica Canyon (Fig. 2) (McGill, 1989). Over most of the Pacific Palisades area the terrace inner edge, which represents sea level at the time of terrace formation, occurs at an elevation of 71–85 m (McGill, 1989). Regionally, the wave-cut platform dips ~1° seaward, although locally it may be deformed by north-northeast– to east-trending, short-wavelength folds (500–1000 m) and dip as steeply as 6°–14° (McGill, 1989). A combination of amino acid racemization results (Wehmiller et al., 1977; Lajoie et al., 1979) and paleontologic data (Woodring, *in* Hoots, 1931; G. Kennedy, 1977, written commun., cited *in* McGill, 1989) indicates that the terrace developed during the oxygen isotope stage 5e sea-level highstand ca. 125 ka (McGill, 1989). Studies elsewhere in California suggest that the stage 5e terrace actually formed late during this highstand, ca. 117–120 ka (Rockwell et al., 1992; Muhs et al., 1992, 1994; Rockwell, 1994). At Point Dume, 25 km to the west, the inner edge of the terrace occurs at an elevation of only ~25 m (Birkeland, 1972; McGill, 1989; Weber, 1992).

Geomorphology of the Santa Monica Fault Zone Onshore

The most recently active trace of the Santa Monica fault onshore is marked by a series of south-facing scarps that extend 11.5 km from the west Beverly Hills lineament north of Century City, westward through west Los Angeles, Westwood, Santa Monica, and Pacific Palisades, where the fault trends offshore at Potrero Canyon (Fig. 2). In contrast to the mountain-front location of the Hollywood fault, the Santa Monica fault scarps are 3–4 km south of the topographic mountain front. The presence of the deeply dissected old alluvial fans between the active fault and the mountain front and the conspicuous lack of active alluvial fans at the mountain front suggest relatively little, if any, recent uplift along any faults at the mountain front. In contrast, apices of young fans along the well-defined scarp imply that most recent deformation is occurring along these scarps.

Some earlier maps (e.g., Crook et al., 1983) show the Santa Monica fault extending eastward across the alluvial plain south of Beverly Hills and Hollywood. East of the west Beverly Hills lineament, however, no geomorphologic evidence of recent surficial fault activity is seen in the gently sloping alluvial plain along strike of the Santa Monica fault. This suggests that the Santa Monica fault, at least in its most recent incarnation, does not extend east of the west Beverly Hills lineament as a surficial feature.

A nearly continuous, N60E-trending scarp characterizes the easternmost 3 km of the Santa Monica fault. The scarp extends along the northern edge of Santa Monica Boulevard, which was originally built as a trolley line that followed the natural break in slope provided by the scarp; a major bend in the boulevard south of Westwood follows a bend in the scarp. The scarp height along this reach ranges from 7 to 12 m. West of the major bend south of Westwood the fault trends ~N70E for ~600 m to the eastern edge of the 925-m-wide drainage of Sepulveda Canyon, where late Holocene erosion and deposition have obscured the scarp. The large Sepulveda fan is to the south of the fault; lines drawn on the fan surface perpendicular to contours converge on the fan's apex, which is located approximately at the fault crossing of the Sepulveda drainage (Fig. 2). The scarp reappears on the west side of the Sepulveda fan near the southwest corner of the West Los Angeles Veteran's Administration Hospital grounds. The scarp height increases westward as onlapping distal Sepulveda fan deposits thin westward away from the fan apex.

The central reach of the fault, between Interstate Highway 405 and the coast, exhibits three distinct, left-stepping, en echelon scarps (Fig. 2). The eastern two scarp segments trend generally N70E, whereas the western segment changes trend westward, from N60E to N80W. Scarp heights typically range from 8 to 12 m for the two eastern scarps, although at the terminations of individual segments the scarp heights decrease to zero. The three en echelon segments overlap by as much as 750 m. This overlap, as well as the lateral decrease in scarp height on the individual segments toward their terminations, is especially well illustrated along Bundy Drive in Santa Monica, where the two eastern segments overlap. The spacing between the two overlapping segments there, measured perpendicular to fault strike, is ~300 m. West of the western end of the easternmost en echelon segment (near the corner of Bundy Drive and Wilshire Boulevard), the scarp projects into the anomalous, N80W-trending Brentwood Knoll and its N80E- to west-trending western extension (Fig. 2). This feature, which projects ~25 m above the surrounding alluvium, probably represents an anticlinal ridge developed above a shallow blind thrust fault that may be a westward continuation of the easternmost en echelon segment.

The westernmost en echelon scarp is broader than the other two, but its total relief (~10 m) is similar to that of the scarps to the east. This results in the western scarp being more subdued topographically than the two eastern segments. The surface slope of the western scarp shallows westward, and the scarp is >300 m wide at its western end at Santa Monica Canyon (Fig. 2). To the west of Santa Monica Canyon two distinct 3–5-m-high scarps extend across the broad marine terrace along the projected trace of the fault. These scarps project directly into the Potrero Canyon exposure of the fault (Fig. 2). It is not clear, however, whether these features are fault scarps or terrace risers associated with Pleistocene(?) fluvial terraces inset into the stage 5e marine terrace. Thus, their presence along the trace of the fault may be simply coincidental.

POTRERO CANYON STRAND OF THE SANTA MONICA FAULT

The Potrero Canyon fault, recognized as part of the Santa Monica fault zone by McGill (1989), was first reported by Hoots (1931) on the basis of exposures at the mouth of Potrero Canyon. Although the fault is no longer visible in the sea cliff there, annotated photographs taken in 1932 (Johnson, 1932) reveal a single strand striking N75E and dipping 45°–55°N at the base of the canyon (data summarized in McGill, 1989). The fault splays upward into a near-vertical strand and a more southerly, north-dipping strand (Johnson, 1932; Hill, 1979; Hill et al., 1979; McGill, 1989). McGill's (1989) detailed mapping of the area shows that maximum vertical separation has occurred on the vertical splay, although beds are also folded and separated in an up-to-the-north sense by the north-dipping strand (Hill, 1979; McGill, 1989). Hoots (1931) suggested that movement began on the

Potrero Canyon fault after deposition of upper Pliocene or lower Pleistocene beds but before deposition of uppermost Pleistocene alluvial deposits. North-side-up vertical separations decrease upward in progressively younger alluvial strata above the upper Pleistocene marine-terrace deposits; the youngest sediments near the top of the canyon walls are vertically displaced only ~1.3 m across the vertical strand (Johnson, 1932; Hill, 1979). Johnson (1932) reported that individual strands of the vertical splay reach the ground surface, although McGill (1989) could only trace the fault to within 4 m of the ground surface.

Displacement of the ca. 120 ka oxygen isotope stage 5e marine terrace deposits at the mouth of Potrero Canyon provides a rate of vertical uplift across the Santa Monica fault system. McGill (1989) correlated the wide stage 5e terrace at ~60 m elevation in the hanging wall of the fault with marine terrace deposits at an elevation of ~6 m in the footwall. The stage 5e terrace in the hanging wall exhibits a warm-water fauna typical of this highstand (Wehmiller et al., 1977; Lajoie et al., 1979; Weber, 1992). In contrast, a long-unexposed locality in the footwall terrace contains some forms that may indicate a cooler water fauna (D. Ponti, 1996, personal commun.), thus calling McGill's correlation into question. Nevertheless, in the absence of definitive evidence based on redating the footwall terrace deposits, provisional acceptance of McGill's original correlation of the footwall terrace with the stage 5e terrace seems appropriate.

Terrace inner edge elevations of 71–85 m over most of the Pacific Palisades area (McGill, 1989) indicate a late Pleistocene–Holocene uplift rate of ~0.6–0.7 mm/yr. Most of this uplift is related to reverse slip on the Santa Monica fault. At Potrero Canyon the marine terrace exhibits ~29 m of north-side-up separation along the vertical fault strand; vertical separation on the north-dipping strand is ~5 m (Johnson, 1932; McGill, 1989). Including warping within a few tens of meters of the fault, total vertical separation of the terrace deposits across the Potrero Canyon strand is ~55 m (see Plate 2 of McGill, 1989). Thus, the average late Pleistocene–Holocene uplift rate across the fault is ~0.5 mm/yr. Correction for the 45°–55° dip of the fault yields a reverse-slip rate of ~0.6 mm/yr. This slip rate is based solely on vertical separations in the sea-cliff exposure; it does not take into account any left-lateral slip on the fault system (discussed herein), and therefore represents only the minimum average late Pleistocene–Holocene slip rate for the Santa Monica fault system, assuming that the footwall and hanging-wall terrace deposits have been correlated correctly.

If the footwall marine terrace is associated with oxygen isotope stage 5e, then the footwall block south of the Potrero Canyon fault also appears to have been uplifted, albeit at a much slower rate than the hanging wall. South of the zone of near-fault warping, the gently south sloping surface of the abrasion platform at the base of the terrace gravels crops out at 6 m elevation (McGill, 1989). The most widely accepted value for mean sea level during the oxygen isotope stage 5e high stand is +6 m (e.g., Bloom et al., 1974; Chappell, 1983). The inner edge of the terrace is located 1850 m north of the mouth of Potrero Canyon (measured perpendicular to fault strike). Overall, the terrace dips slightly $<\sim 1^\circ$ to the south, and in the hanging wall just north of the fault, the abrasion platform is ~20 m lower than the elevation of the inner edge (McGill, 1989). This suggests that during the stage 5e highstand, the abrasion platform currently exposed in the hanging wall at the mouth of Potrero Canyon was at an original elevation of ~–20 m below sea level (this is similar to the present −15 m depth of the seafloor 1850 m offshore Potrero Canyon; Dibblee, 1992). Correcting to present-day sea level by adding 6 m to the −20 m value yields an expected present-day elevation in the footwall at the mouth of Potrero Canyon of ~–14 m below sea level, if there has been no Santa Monica fault–related uplift. The actual +6 m elevation of the abrasion platform at the canyon mouth indicates that the site has been uplifted ~20 m during the past 120 k.y. This in turn indicates a slow uplift rate of slightly <0.2 mm/yr for the coastline south of the Potrero Canyon fault. This rate is similar to the rate calculated on the basis of estuarine sediments recovered from geotechnical boreholes excavated at a site 3 km east of Potrero Canyon, ~300 m south of the Santa Monica fault (Converse Consultants Report, 1998). These sediments, which are interpreted to correlate with sea level during the stage 5e highstand, were recovered from 25 m elevation. This indicates an uplift rate of ~0.2 mm/yr. The similarity of the uplift rates calculated at the two sites suggests that this is a regional effect in the footwall of the Santa Monica fault.

If the footwall terrace at Potrero Canyon actually formed during oxygen isotope stages 5a or 5c, complete preservation of the 5e terrace in the hanging wall implies that the footwall terrace inner edge was probably located at the fault, and the terrace may have reoccupied the footwall part of the older stage 5e terrace. Sea level during oxygen isotope stage 5a was ~–2 to −5 m below sea level, whereas sea level during stage 5c was probably ~–2 m below sea level (Rockwell et al., 1992; Muhs et al., 1992, 1994; Rockwell, 1994). Thus, if the footwall terrace formed during stage 5a, then ~7−10 m of uplift has occurred during the past 77–80 k.y. This yields a very slow footwall uplift rate of ~0.1 mm/yr. If the footwall terrace developed during oxygen isotope stage 5c, then ~7 m of uplift occurred during the past 102–104 k.y., yielding an even slower footwall uplift rate of <0.1 mm/yr. Thus, even if the footwall terrace is a younger terrace (e.g., stage 5c or 5a), it will only increase the rate across the Santa Monica fault by ~0.1 mm/yr, with a correspondingly small increase in reverse slip rate.

OFFSHORE EXTENSION OF THE SANTA MONICA FAULT ZONE

West of Potrero Canyon, the Santa Monica fault extends offshore parallel to the coast to near Point Dume (Fig. 4). South of Malibu, Vedder et al. (1986) used seismic reflection profiles spaced 1–7 km apart to map two parallel strands of the fault (their Malibu Coast fault), ~500 m apart, that trend east-west ~2−3.5 km south of the coast; both strands have seafloor expression and cut strata of presumed Holocene age. Junger and Wagner (1977) also used seismic reflection profiles, from a somewhat denser data grid with an average line spacing of 2–4 km, to map a single narrow zone of offshore faults south of the Malibu coast (Fig. 4). Junger and Wagner (1977) showed that the Santa Monica fault zone (their Dume fault), westward from the coast, consists of two or more parallel strands that cut strata that vary in age from late Pliocene to Quaternary. The quality of their data did not allow recognition of each fault on every profile, and thus they were unable to create a complete, detailed map of the offshore part of the fault zone. At the intersection of the Palos Verdes fault south of Point Dume (discussed herein), they could not locate the Santa Monica fault reliably because of poor data. They noted, however, that the Santa Monica fault appears to have a left-lateral offset south of Point Dume, active deformation stepping southwestward to the Anacapa-Dume fault (our terminology; Fig. 4).

In general, where best located south of Malibu, the seafloor traces mapped by Junger and Wagner (1977) and Vedder et al. (1986) are similar in location and orientation, although to the east of Malibu the Junger and Wagner (1977) fault trace trends slightly more northeastward than the trace shown by Vedder et

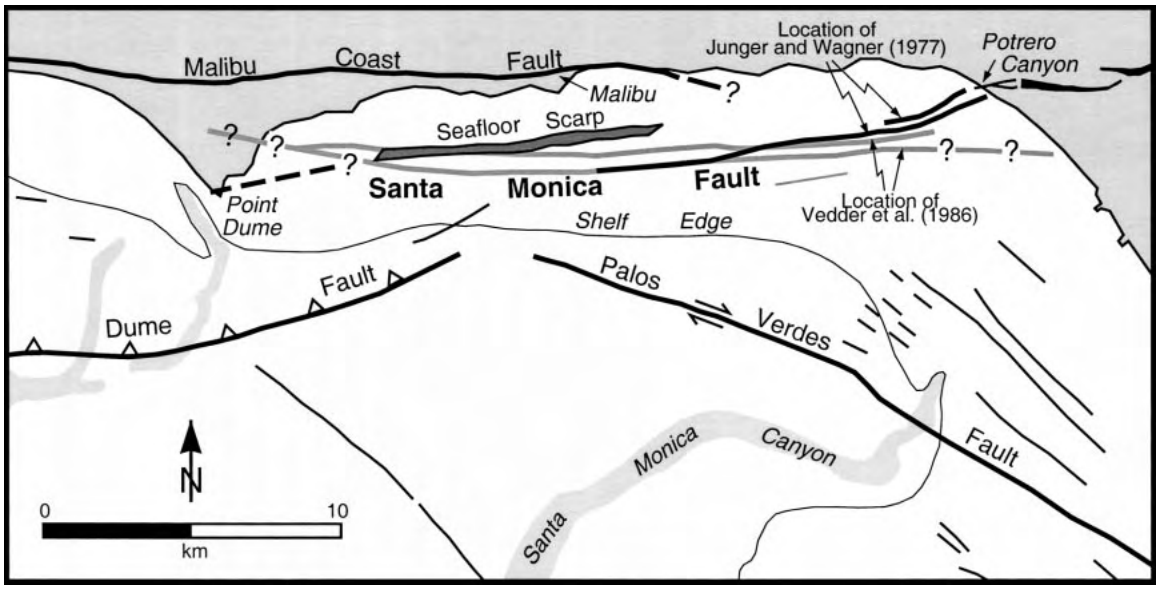

Figure 4. Map of active surficial faults along the Malibu Coast. Note differing locations for offshore Santa Monica fault shown by Junger and Wagner (1977) and Vedder et al. (1986), as well as 10-m-high, south-facing submarine scarp south of Malibu. Thick lines denote faults discussed in the text. Thinner lines show other faults that exhibit either Holocene or Pleistocene activity. Stipple denotes submarine canyons. Data are compiled from Junger and Wagner (1977) and Vedder et al. (1986).

al. (1986). Bathymetric data from the Malibu shelf reveal the presence of a 10-m-high, south-facing scarp at 30–40 m depth 5 km south of the coast (Fig. 3). The submarine scarp, which trends slightly more northeastward than the Vedder et al. (1986) scarps, cannot be traced eastward into shallower water depths of the Santa Monica shelf, where it presumably has been obliterated by storm waves. The scarp may be the seafloor scarp of the Santa Monica fault. Alternatively, it may be a submerged sea cliff associated with an ancient sea-level highstand.

Junger and Wagner (1977) depicted the fault zone connecting with the onshore Santa Monica fault at Potrero Canyon. In contrast, Vedder et al. (1986) portrayed their southern Santa Monica fault strand extending onshore 2 km south of the Potrero Canyon landfall. Their data coverage, however, does not extend to within 5 km of either the eastern (Point Dume) or western (Potrero Canyon) landfalls of the fault, and thus their nearshore fault locations are best viewed as speculative extrapolations of their locations farther offshore. Their mislocation of the landfall in Santa Monica was probably based on connecting their well-determined offshore fault locations south of Malibu with the landfall of the Santa Monica fault shown on older maps, which were based on projecting the inactive southern strand of the fault to the surface.

Vedder et al. (1986) drew the Santa Monica fault extending onshore north of Point Dume, presumably as the Paradise Cove fault (Fig. 4). Dibblee (1993), however, showed that this fault does not cut older alluvium. This observation suggests that the Paradise Cove fault is probably not the western continuation of the Santa Monica fault, which cuts strata of this age farther to the east. However, a major, steeply dipping fault exposed at the southern tip of Point Dume may represent a western strand of the Santa Monica fault (dashed line in Fig. 4). The Santa Monica fault is difficult to trace west of Point Dume. Vedder et al. (1986) mapped two isolated offshore faults that cut Pleistocene strata approximately along trend with the Santa Monica fault west of Point Dume (Fig. 4). They did not report any through-going faults in this area, however, and the Santa Monica fault may terminate near Point Dume.

PALEOSEISMOLOGY OF THE SANTA MONICA FAULT

Previous Investigations

Prior to this study the current state of activity of the Santa Monica fault was unknown; displacement of alluvial deposits younger than oxygen isotope stage 5e (ca. 120 ka) at Potrero Canyon provided the only information on the age of most recent fault motion (Johnson, 1932; Hill, 1979; McGill, 1989). In the absence of evidence for Holocene activity, the fault is not zoned as active by the State of California, although the City of Santa Monica requires detailed fault studies within defined seismic risk zones.

The eastern en echelon segment of the central Santa Monica fault zone was excavated at two sites during the early 1980s (Crook et al., 1983; Crook and Proctor, 1992). Although these studies revealed some near-surface faulting, the results concerning Holocene activity were inconclusive, largely because of the scarcity of datable material in the trenches. As a consequence, the common public perception has been that the fault is inactive. Because of this perception and the lack of fault zonation, new building in some jurisdictions continues directly atop the most recent surface trace of the fault zone.

One strand of the Santa Monica fault was exposed in a building excavation at the southwest corner of Wilshire Boulevard and Bundy Drive in west Los Angeles (Fig. 2) (G.A. Brown, 1993, personal commun.). By the time this fault was discovered at 6 m depth, however, the shallower parts of the excavation were already cemented over, and no useful paleoseismologic data were recovered. Groundwater was encountered at this site at a depth of 21 m; a second excavation at the northwest corner of the intersection encountered groundwater at a depth of only 5 m (G.A. Brown, 1993, personal commun.), indicating that the fault there acts as an effective groundwater barrier.

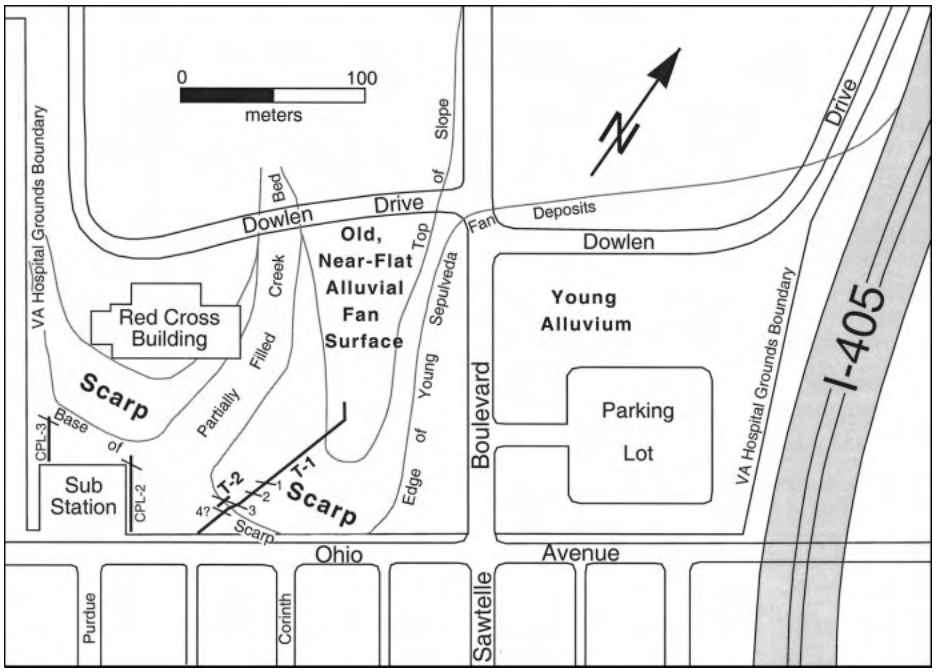

Figure 5. Detailed map of Veteran's Administration trench site in west Los Angeles showing major geomorphic features and locations of trenches T-1 and T-2. Location is shown in Figure 2. Numbered lines crossing trenches show locations and strikes of the four largest faults. Locations of creek and scarps adjacent to trench site are from 1927 Fairchild air photo; artificial fill emplaced during construction of Red Cross building has largely obliterated the creek and fill has been added to the upper part of the scarp south of Red Cross building to create a building pad. CPL-2 and CPL-3 denote locations of earlier paleoseismologic trenches excavated by Crook et al. (1983; Crook and Proctor, 1992); short lines show strikes of steeply dipping faults exposed in those trenches.

This Study

We excavated two trenches (T-1 and T-2) across the well-defined scarp at a site near the southwestern corner of the Veteran's Administration Hospital Grounds in west Los Angeles (Fig. 5). The site is located at the eastern end of the eastern en echelon segment, along the western edge of the Sepulveda alluvial fan ~250 m west of Interstate 405 and ~75 m east of the eastern trench site S-2 of Crook et al. (1983; Crook and Proctor, 1992). The scarp is truncated by recent fluvial erosion and alluvial fan deposition 25 m east of the trench site. At the trench site the scarp is 5 m high and has a south-facing surface slope of 5°–6°. The base of the scarp is marked by a sharp inflection point with the young, gently dipping (1°–2°SW) sediments of the distal Sepulveda fan. The top of the scarp is also defined by a sharp inflection point between the scarp slope and the gentle southward slope of the dissected alluvial surface to the north. Human changes to the topography of most of the site have been minimal, although a N15°E-trending stream channel located ~50 m west of our trenches has been partially infilled to create a parking lot, and fill has been added to the upper part of the scarp to the west of the stream channel to create a building pad.

Trench T-1 extended 112 m across the entire topographic fault scarp (Fig. 6). The southern edge of the trench was located 20 m south of the base of the topographic scarp in late Holocene Sepulveda fan alluvium. The continuity of the trench is interrupted between 16.5 and 18.5 m north of its southern end and

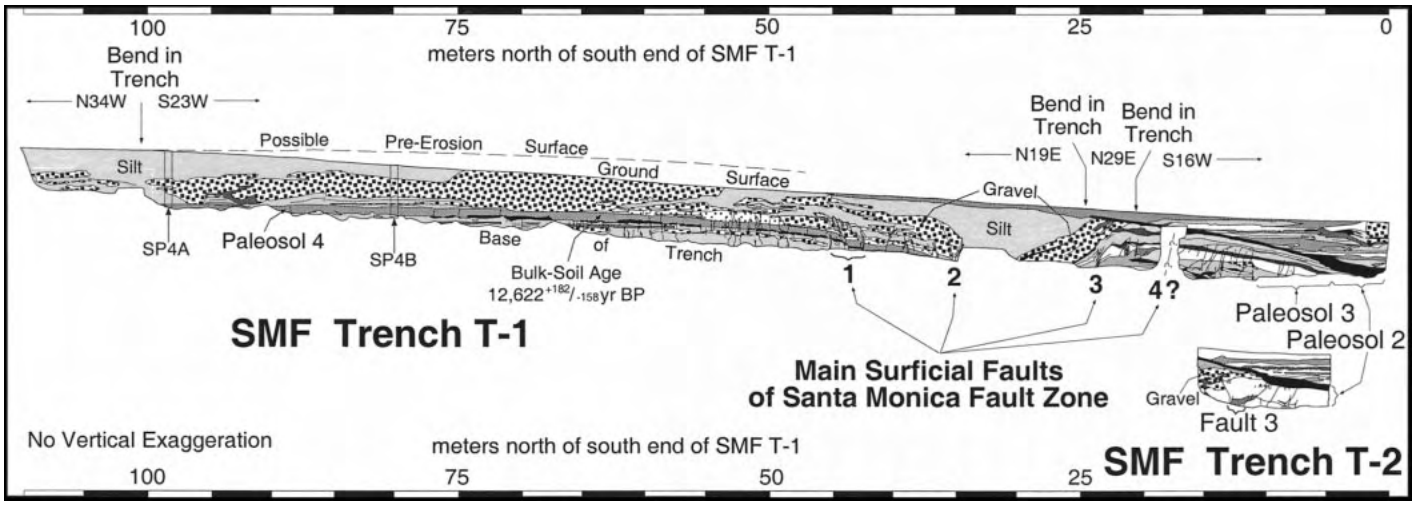

Figure 6. Logs of trenches T-1 and T-2. Note south-dipping sequence onlapped by late Holocene Sepulveda fan strata near south ends of trenches and major disruption of prominent gravel bed by faults 2 and 3. Pre-erosion surface is based on extrapolation of paleosol 4 surface to ground surface southward from 100 m north. No vertical exaggeration.

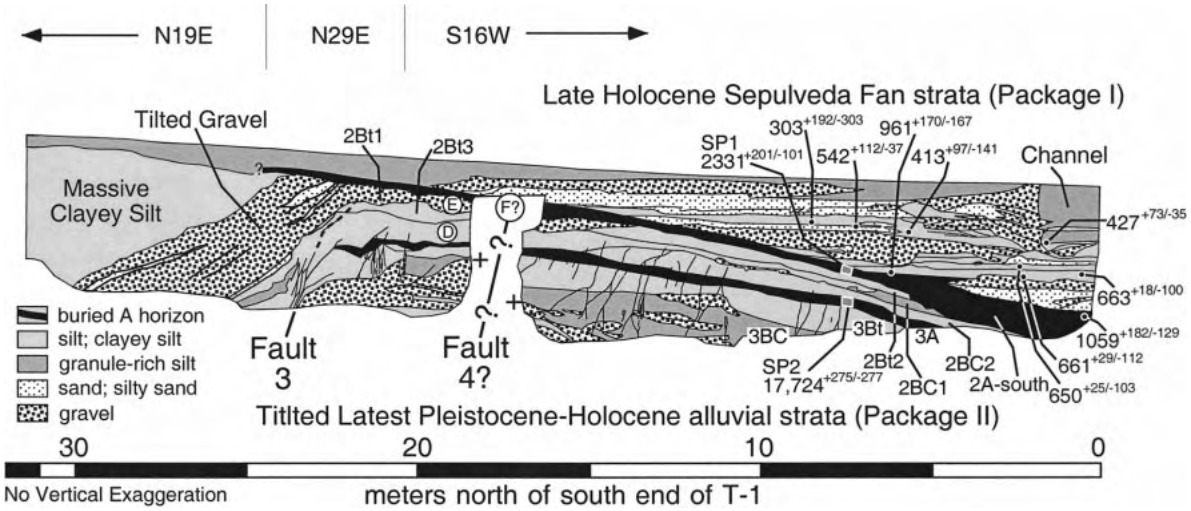

Figure 7. Detail of southern part of trench T-1 log showing south-dipping package II strata onlapped by flat-lying, late Holocene Sepulveda fan strata of package I. Soil horizons within paleosols 2 and 3 are denoted by, e.g., 2A, 3Bt, 3BC1. See text for discussion. The A horizons of buried paleosols 2 and 3 are highlighted in black. Circled letters show locations of structural and/or stratigraphic features used to interpret paleosurface ruptures. Gray boxes show locations of bulk-soil samples from soil profiles 1 and 2 (SP1 and SP2). Remainders of soil profiles are not shown for clarity. Plus symbols denote top of a granule-pebble gravel layer displaced by postulated fault 4. No vertical exaggeration.

below 1 m depth by an east-west electrical conduit. All measurements herein refer to distance north of the southern edge of trench T-1 in meters (e.g., electrical conduit occurs at 16.5–18.5 m north). Trench T-2 was a short (11 m) trench excavated parallel to and 5 m west of T-1 at the extrapolated location of a major fault (Fig. 5). Unless otherwise noted the following descriptions refer to trench T-1. After scraping the trench walls smooth, we surveyed the three-dimensional location of several thousand selected data points. Using these points as a reference grid, we mapped the trenches at a scale of 1:20.

Stratigraphic, Soil, and Age Data

Trench T-1 exposed generally south-dipping alluvial strata that have been locally complexly deformed by folding and faulting (Fig. 6). In order to interpret the paleo-earthquakes that caused this deformation, we must first consider in detail the stratigraphic and age relationships of the deposits exposed in the trenches. We have divided T-1 into four distinct packages, based on internally consistent stratigraphy, structures, and soil development. These four packages are, from south to north: (1) flat-lying Sepulveda fan strata; (2) south-tilted alluvial strata that are onlapped by the flat-lying strata; (3) a zone of structural complexity between 22 and 34.5 m north; and (4) the northernmost 75 m of the trench, which exhibits a very broad, gentle anticlinal warp.

Package I

The flat-lying alluvial strata of unit 1 consist of well-bedded, friable gravel, sand, and silt (Fig. 7). Although some beds are locally channeled and discontinuous, many beds are traceable continuously from the southern edge of the trench to the point at which they onlap the south-dipping strata of package II. There is virtually no soil development within package I, and the surface soil exhibits only a 15-cm-thick A horizon. The lack of pedogenesis is consistent with our interpretation that these sediments are rapidly deposited Sepulveda alluvial fan strata.

Package I Age Control. Accelerator mass spectrometer (AMS) radiocarbon age analyses of nine samples of detrital charcoal from package I yielded late Holocene ages, from A.D. 891 $^{+129}/_{-182}$ to A.D. 1651 $^{+303}/_{-192}$ (Table 1). In general, age dates decrease progressively upsection; the exception was a sample that yielded an age of A.D. 1408 $^{+37}/_{-112}$ (7 m north, 1.35 m depth) from a deposit that also contained the sample with an age of A.D. 1651 $^{+303}/_{-192}$ (8 m north, 1.4 m depth). Three samples collected from a clayey silt layer at 2.6 m depth at the south end of the trench yielded nearly identical dates of A.D. 1300 $^{+103}/_{-25}$, A.D. 1289 $^{+112}/_{-29}$, and A.D. 1287 $^{+100}/_{-18}$ from different labs (unless otherwise noted all ^{14}C samples were dated using the AMS technique at either the Lawrence Livermore Laboratory or ETH in Zurich; corrected, calendar ages are quoted with 2 σ errors [95% confidence limits]; Table 1).

Package II

Package II consists of gently south-dipping (~15°S) silt, sand, and gravel beds similar to the flat-lying alluvial fan strata of package I (Fig. 6). The top of the dipping sequence projects northward to match the surface slope of the scarp north of ~30 m north. Package II encompasses two buried soils, paleosol 2 (younger) and paleosol 3 (older) (Appendix Table A1). Due to the onlapping nature of the flat-lying strata, the burial age of paleosol 2 decreases northward; north of ~28 m north paleosol 2 merges with the active surface soil (soil 1), which is discussed below as part of package IV. In general, the tilted strata are markedly continuous laterally. The tops and bases of two gravel channels exposed within the dipping sequence are elongate parallel to the dip direction. This relationship is best illustrated by a 5–15-cm-thick, granule to small pebble gravel bed exposed from 9.2 to 11.3 m north at 2.6 m depth. These observations indicate that the south-dipping strata were originally deposited horizontally and have subsequently been tilted.

Three beds within package II provide important limits on paleo-earthquake timing, and we discuss them in detail here. The argillic horizon of paleosol 2, which is lithologically controlled over most of its length (21.5–5.5 m

TABLE 1. RADIOCARBON SAMPLES AND AGES

Sample number	Beta lab number	Reactor lab number	^{14}C age (yr B.P. ± 1σ)	Corrected ^{13}C age (yr B.P. ± 1σ)	Calendric age (2σ)
TKR C-1	Beta-57044	CAMS-4304	1070 ± 70		A.D. 989 +167/–170 (A.D. 819–1156)
SMF T1–1	Beta-57045	CAMS-4305	1150 ± 70		A.D. 891 +129/–182 (A.D. 709–1020)
SMF T1–3	Beta-57052	ETH-9807	655 ± 55		A.D. 1289 +112/–29 (A.D. 1260–1401)
SMF T1–4	Beta-57046	CAMS-4306	670 ± 50		A.D. 1300 +103/–25 (A.D. 1275–1403)
SMF T1–9	Beta-57053	ETH-9808	660 ± 50		A.D. 1287 +100/–18 (A.D. 1269–1387)
SMF T1–24	Beta-57054	ETH-9809	320 ± 55		A.D. 1523 +35/–73 (A.D. 1450–1558)
SMF T1–25	Beta-57047	CAMS-4307	320 ± 70		A.D. 1530 +148/–90 A.D. 1537 +141/–97 (A.D. 1440–1678) A.D. 1635 +43/–195
SMF T1–28	Beta-57055	ETH-9810	535 ± 50		A.D. 1408 +37/–112 (A.D. 1296–1445)
SMF T1–29	Beta-57048	CAMS-4308	270 ± 70		A.D. 1651 +303/–192 (A.D. 1459–1954)
SMF T1 2A (bulk MRT)	Beta-63639	CAMS-7654		2290 ± 70	381 B.C. +101/–201 (582–280 B.C.)
SMF T1 3A (bulk soil)	Beta-63640	CAMS-7655		14 820 ± 100	15 774 B.C. +277/–275 (15 497–16 049 B.C.)
SMF T-1.3 (bulk soil)	Beta-69087	CAMS-10737	10 700 ± 60	10 690 ± 60	10 672 B.C. +158/–182 (10 514–10 854 B.C.)
SMF T2–3	Beta-57056	ETH-9811	440 ± 50		A.D. 1442 +80/–41 (A.D. 1367–1522)
SMF T1–3 and T1–9 averaged values:					A.D. 1288 +106/–117 (A.D. 1171–1394)
SMF T2–15	Beta-57050	CAMS-4309	220 ± 70		A.D. 1666 +289*/–155 (A.D. 1511–1955)

Notes: Calendar ages calculated using CALIB 3.0 (Stuiver and Reimer, 1993; method A unless otherwise noted). Calendric ages for T1–3, T1–9, T1–24, T1–25, T1–28, and T2–3 are weighted ages for multiple intercepts using method B. CAMS—Lawrence Livermore National Laboratory; ETH—Eidgenossische Technisch e Hochschule.

north), has developed through a 25–50-cm-thick bed (units 2Bt1 and 2Bt2 in Fig. 5) that exhibits marked lateral changes in grain size, despite on an overall laterally constant thickness. The northern third of this deposit (15–21.5 m north) consists of poorly sorted, granule to large pebble gravel composed of ~50% clasts and ~50% sandy, clayey silt matrix. Almost all of the clasts consist of Santa Monica Slate, which is exposed in the Santa Monica Mountains 4 km north of the trench site (Dibblee, 1991). At 15 m north, the percentage of gravel-sized clasts decreases abruptly to ≤5% across a gradational, but relatively sharp, near-horizontal contact. To the south of 15 m north, the deposit consists of sandy, clayey silt, with variable, but minor (typically ~3%−5%), amounts of granules and small pebbles. The southern part of the deposit is lithologically indistinguishable from the matrix of the northern part of the bed. Thus, the coarse-grained northern third of the bed forms a wedge-shaped gravel lens (2Bt1 in Fig. 7). At its northern end the gravel merges across a poorly defined contact with a lithologically identical, north-dipping gravel deposit (package III, discussed in the following).

The bed below the gravel wedge also defines a southward-thinning wedge, although the lower bed is composed of sandy silt. The northern end of this deposit encompasses unit 2BC1 as well as the lowest part of the argillic horizon (unit 2Bt3) between 18.5 and 23.5 m north. The northern 3 m of the bed (19.5–22.5 m north) is 110−120 cm thick. At ~14 m north the bed thins southward to <25 cm thickness (Fig. 7). The southern part of this bed is separated from the underlying, lithologically similar silt bed by the several thin gravel beds, including the 5–15-cm-thick gravel bed exposed from 9.2 to 11.3 m north at 2.6 m depth. The northern edge of the 2BC1–2Bt3 silt wedge is a steeply north dipping fault contact (described in the following) that juxtaposes the silt with an interlayered sequence of north-dipping silt and granule-gravel beds. We discuss the paleoseismologic significance of the two wedge-shaped package II deposits in the following.

The third important bed in package II is the silt bed that represents the A horizon of paleosol 2 (2A in Fig. 7). Stratigraphic relations near the south end of the trench reveal a complex depositional history for this bed. The southern 25 m of unit 2A, which dips parallel to and caps the tilted sequence, maintains a constant 15−25 cm thickness, with the exception of possible structural complexities where it is obscured by the electrical conduit (discussed in the following). South of 7 m north, however, the top of unit 2A diverges from the base of the unit, and becomes parallel to and interfingers with the flat-lying, package I Sepulveda fan beds near the south end of the trench (Fig. 7). In the southernmost several meters of the trench, unit 2A has an erosional basal contact, with a well-developed pebble-cobble lag between 1.5 and 5.5 m north. Underlying units 2Bt2 and 2BC1 are cut out south of 5.5 m north. The base of unit 2A here thus represents the base of a channel eroded into units 2Bt2 and 2BC1. As with several of the channels exposed in package I, the trend of this channel is approximately parallel to the scarp (i.e., perpendicular to the trench).

We interpret the depositional history of unit 2A as follows: (1) horizontal deposition of most of the unit as a sheet-like deposit of relatively constant thickness; (2) tilting of the entire package containing unit 2A and underlying units; (3) downslope transport of sediment eroded off tilted unit 2A; and (4) accumulation of eroded material at the base of the scarp, where it interfingered with contemporaneously deposited Sepulveda fan strata of package I as part of a base-of-slope wedge that onlapped older unit 2A deposits upslope. Hereafter, we refer to this flat-lying, southern part of unit 2A as unit 2A-south.

Package II Age Control. AMS ^{14}C dates on two detrital charcoal samples from the southern part of the trench, one from the base of the south end of the trench, and one from just above the top of the flat-lying part of unit 2A at 6 m north, yield indistinguishable dates of A.D. 891 $^{+129}/_{-182}$ and A.D. 989 $^{+167}/_{-170}$, respectively (Table 1). AMS dating of a bulk soil sample from the A horizon of paleosol 2 from the southern part of the tilted A horizon at 7.5 m north, 2.8 m depth (i.e., north of the post-tilting, base-of-slope wedge 2A-south) yielded a bulk-soil date of 381 $^{+101}/_{-201}$ B.C. (Table 1). This sample is from the same location as our detailed soil profile of paleosol II, labeled as SP (soil profile) 1 in Figure 6 (soil data are described in Table A1). The bulk-soil AMS date represents the average age of disseminated organic carbon within the A horizon. A similar bulk soil sample collected at 7.5 m north, 3.1 m depth from the tilted A horizon of paleosol 3 (SP2) yielded a date of 15 774 $^{+277}/_{-275}$ B.C.

The bulk-soil ages of the package II paleosols provide important limits on the ages of

several paleo-earthquakes (discussed in the following), and we therefore examine the age estimates in detail. A bulk-soil age, when combined with an independent measurement of the mean residence time (MRT) of the organic matter in the paleosol, provides the burial age of the paleosol. Fortunately, the burial age for paleosol 2 can be estimated using the detrital charcoal ages from onlapping package I. As with all detrital charcoal samples, however, we must consider the possibility that the samples are reworked from older deposits.

If the package I detrital charcoal had a near-zero depositional age (i.e., it was burned in a brush fire and deposited within package I soon afterward), then the MRT of organic matter within paleosol 2 is ~1.3 k.y. (381 $^{+101}/_{-201}$ B.C. bulk-soil date minus ~1 ka age of the base of package I). Alternatively, if the package I detrital charcoal were already ~1 k.y. old at deposition and were deposited very recently, then the MRT for paleosol 2 may be as great as ~2.3 k.y. The upward-younging of the detrital charcoal ages from package I suggests that the second possibility is highly unlikely.

Although the general upward age progression of the package I detrital charcoal ages suggests that package I was deposited incrementally, incorporating charcoal that was relatively young at deposition, the presence of the A.D. 989 $^{+167}/_{-170}$ sample from the same horizon that yielded three, near-identical ~650 yr old ages suggests at least limited reworking within the section. The A.D. 989 $^{+167}/_{-170}$ sample was recovered from 2 cm above the contact between the flat-lying, southern extension of unit 2A and the overlying bed, which contains the ~650 yr old detrital charcoal samples. Although the contact between these two units is sharp, it is locally bioturbated. This suggests that the A.D. 989 $^{+167}/_{-170}$ sample could have been moved upward from the upper part of the flat-lying part of unit 2A. The likelihood of reworking, combined with the indistinguishable A.D. 891 $^{+129}/_{-182}$ AMS date of the sample from the base of this part of unit 2A, suggests that the flat-lying part of unit 2A was probably deposited ~1 k.y. ago. Alternatively, the ~1 k.y. old age dates might come from reworked charcoal that was redeposited ~650 yr ago, indicating that paleosol 2 could have been buried as recently as ca. 650 yr B.P. This would yield an MRT for paleosol 2 of ~1.7 k.y. In summary, the probable MRT for paleosol 2 is ~1.3–1.7 k.y., although we favor the shorter time span.

The ca. 650–1000 yr B.P. burial age for paleosol 2 applies only to the site near the south end of the dipping part of unit 2A where we collected the paleosol 2 bulk-soil sample. Diachronous, northward-younging onlap of package II by the flat-lying package I strata indicates that the burial age of paleosol 2 decreases from south to north. The detrital charcoal AMS ages from package I show that the northernmost part of paleosol 2 at ~25 m north was buried no more than a few hundred years ago.

If we assume that when it was buried the organic matter in paleosol 3 had an MRT similar to the ~1–2 k.y. MRT of paleosol 2, then the ca. 17.7 ka age of the paleosol 3 bulk-soil sample suggests burial of paleosol 3 ca. 16–17 ka. Coupled with the ~1 ka burial age for soil 2, these age relations indicate that paleosol 2 required ~15–16 k.y. to develop. This estimate compares favorably with our ca. 15–19 ka soil age estimates for paleosol 2 based on the degree of soil development (soil-development index [SDI] and maximum horizon index [MHI] values) (Table A1; Figures A1 and A2). The degree of soil development (SDI and MHI values) for paleosol 3 suggests that it required ~19–22 k.y. to develop (Table A1).

Package III

Package III encompasses a zone of stratigraphic and structural complexity between 22 and 34.5 m north (Fig. 6). The southern part of package III, between 22 and 30 m north, is dominated by a north-dipping, tabular gravel bed. The gravel is 1.8–2.5 m thick and has relatively planar upper and lower contacts that dip 25°–35°N (Fig. 7). The bed, which consists of clast-supported, granule to large pebble gravel consisting almost exclusively of Santa Monica Slate clasts, is lithologically indistinguishable from the unit 2Bt1 gravel wedge in package II. Sandstone and granule to small pebble stringers within the otherwise massive gravel bed, together with a basal granule lag, are individually traceable for as much as 3.5 m. The stringers are oriented subparallel to the base and top of the gravel bed and do not significantly change thickness laterally, indicating that the gravel was deposited near horizontally and was subsequently tilted. The northern end of package III is a partially faulted contact with another thick gravel bed. These relationships are described as part of package IV. The remainder of package III consists of a thick deposit of massive, clayey silt that is exposed between, and above, the two disconnected gravel bodies between 25 and 43 m north. Although we observed hints of a weakly developed pedogenic stratigraphy within the otherwise massive clayey silt, it was too ill defined to map in detail, and is not shown in Figure 6.

Package III Age Control. The southern part of package III represents a zone of transition between the south-dipping paleosols of package II, and a thick, well-developed surface soil that extends to the northern end of the trench. Although this surface soil is developed within most of package III, our detailed soil analyses were conducted on samples from structurally simpler locations in package IV. Therefore we describe this soil, and its implications for package III age control, as part of package IV.

The relationship between the package II paleosols and the tilted gravel, however, are best described here. The silt bed within which the paleosol 2 A horizon was developed extends northward across the north-dipping package III gravel bed at least as far north as 24.5 m north (Fig. 7). North of that point the silt bed becomes indistinguishable as it merges with lithologically similar deposits of the active surface soil. The silt bed truncates both the top and base of the north-tilted gravel bed, as well as all bedding within the gravel, along a sharp, erosional angular unconformity. Thus, silt deposition postdates tilting of the gravel. In addition, the argillic horizon of paleosol 2 extends across the north-dipping gravel bed without a significant change in either thickness or degree of development from that in package II; well-developed clay films extend down through the north-tilted gravel to a depth of 1.5 m at least as far north as 28.5 m north. These pedogenic data indicate that tilting of the gravel was completed during the early stages of paleosol 2 development, probably well before ca. 10 ka.

Package IV

Package IV contains two main stratigraphic sequences. The lower consists of a sequence of well-bedded silt, sand, and gravel, whereas the upper is dominated by a series of bedded to massive gravel bodies that are locally interbedded with massive silt deposits (Fig. 6). The southern end of package IV is marked by a 2-m-thick gravel bed. This gravel is lithologically indistinguishable from the north-tilted bed exposed at the southern edge of package III, and it is probably the faulted northern extension of the same bed. The southern package IV gravel bed dips gently southward and is overlain by the northern part of the massive clayey silt deposit described in package III.

The lower, well-bedded part of package IV defines a very gentle anticlinal warp; strata in the southern part of the package dip gently

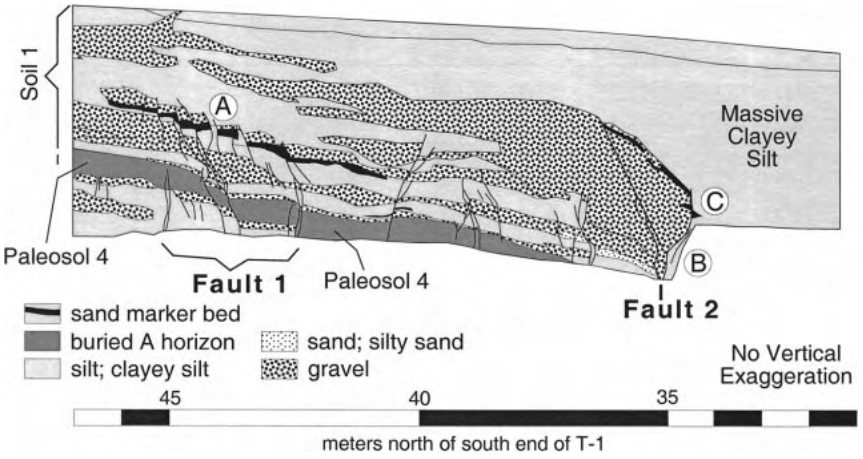

Figure 8. Detail of central part of trench T-1 showing deformation associated with faults 1 and 2. Circled letters show locations of structural and/or stratigraphic features used to interpret paleo-surface ruptures. No vertical exaggeration.

southward, strata from 65 to 85 m north dip near horizontally, and strata in the northern part of the package dip very gently northward (≤1°). The change from horizontal to a gentle northward tilt broadly corresponds to the topographic inflection point at the top of the scarp, which is at ~100 m north (Fig. 6). The top of the well-bedded unit diverges from the surface slope north of ~60 m north, however, suggesting erosion of as much as 2 m of material from the northernmost several tens of meters of the scarp.

Package IV Age Control. North of ~25 m north the surface soil (soil 1) is much better developed than it is to the south, where paleosol 2 is buried, and the very weakly developed active surface soil records no more than a few hundred years of development. We conducted two analyses of soil 1: one at 97.5 m north (SP4A) in a relatively fine-grained section, and one at 79.7 m north (SP4B) in a coarser grained section. The SP4A site yielded a soil age estimate of ca. 48 ka, whereas the SP4B site yielded an estimate of ca. 16 ka; both of these estimates have very large error bars due to the scarcity of well-dated, coastal soils available for comparison (Table A1). Because the only well-dated comparison soils are fine grained, we have a much higher level of confidence in the age estimate from the SP4A site. Furthermore, convergence of the top of well-bedded sequence at the base of package IV with the present ground surface south of 100 m north suggests that ~1 m of material has been eroded from the site of the SP4B profile, whereas the SP4A site appears to be uneroded (Fig. 6). The generally well-developed nature of the surface soil (well-developed clay films extending throughout a several-meter-thick argillic horizon) supports the longer period of development recorded at site SP4A. Thus, soil 1 development north of 25 m north probably encompasses the entire time span recorded by the very weakly developed package I surface soil, paleosol 2, and probably most, and possibly even all, of paleosol 3 south of this point.

This observation conflicts with a 10672 $^{+158}/_{-182}$ B.C. bulk-soil date collected at 63 m north from the A horizon of a very weakly developed paleosol (buried A horizon only; paleosol 4 in Fig. 6) that extends from 35 to 100 m north at ~2.5−4.2 m depth (Table 1). We suggest that this apparent contradiction is explained by evidence for illuviated clay associated with soil 1 development extending down through the paleosol 4 A horizon. We postulate that young organic matter has also been added to the paleosol 4 profile since it was buried, yielding an anomalously young MRT age.

In summary, the paleosol 3 surface in the southern part of the trench and the present ground surface in the northern part of the trench may be segments of a once-continuous paleofan surface that has been displaced by surface faulting. Alternatively, the combined ages of paleosol 2 (ca. 15–19 ka) and paleosol 3 (ca. 19–22 ka) may record a time span shorter than soil 1 development, in which case the paleofan surface correlative with the present ground surface in the northern part of the trench may be beneath paleosol 3 in the southern part of the trench.

The long time interval represented by soil 1 development north of 25 m north (at least several tens of thousands of years) has important implications for our age estimates of some paleo-earthquakes (discussed in the following). For example, on first examination, the massive silt deposit exposed above the north-tilted package III gravel bed would appear to have been deposited against the tilted gravel, and therefore after burial of paleosol 3, which does not extend across the tilted gravel. The long duration of soil 1 development we propose precludes this interpretation, and requires that structures developed in packages III and IV be much older than structures that extend up to similar depths in package II.

Evidence for Faulting

Trench T-1 reveals abundant evidence for faulting. In addition to the structural complexities of package III and the southward tilting of package II, the trench is cut by ~100 steeply dipping faults and fractures (Fig. 6). Although isolated faults and fractures are present as far north as 85 m north, they are much more abundant between 7 and 68 m north. Most of the faults and fractures dip steeply (65°–90°) northward, although a few dip steeply southward; dips ≥80° predominate. Fault strikes range from northwest to northeast; most faults strike east-northeast. None of the faults cuts the onlapping, flat-lying late Holocene deposits, and in the southern part of the trenches many of the cracks terminate near the base of the paleosol 2 argillic horizon.

Stratigraphic evidence for strike-slip motion is common on many faults. Specifically, abrupt changes in bed thickness across faults and lateral terminations of beds at faults require strike-slip juxtaposition of beds that vary laterally in thickness (e.g., lenticular channels). Furthermore, some faults, particularly those in well-bedded parts of the trench, exhibit opposite senses of vertical separations of beds at different stratigraphic levels (e.g., beds cut by fault at 40.5 m north in Fig. 8). We interpret the opposite senses of vertical separation of these beds, as well as the overall very steep fault dips and nonsystematic variations in the amount of displacement up the trace of some faults, as evidence for predominantly strike-slip displacement, with subordinate, and locally variable, vertical components of motion.

The faults and fractures, which were particularly well expressed in the fine-grained parts of the trenches, became more apparent after several days exposure because the sediment adjacent to the faults and fractures dried out more quickly than the unfractured surrounding sediment. In the fine-grained deposits, most of the faults also exhibited a halo of gray, reduced-iron staining within the surrounding

predominantly yellow-brown to brown, oxidized deposits. Some faults were also defined by stringers of exotic material, typically only a few millimeters thick, derived from adjacent beds. We could not confidently ascribe any of these examples to filling of open surficial fractures. In most cases it was impossible to trace faults from fine-grained beds into gravel layers, even in well-bedded intervals where fault separations were well defined stratigraphically above and below the gravel bed. In a few cases, however, faults could be traced through gravel beds by following planar alignments of pebbles along the fault trace. Only a few of the largest faults have gouge zones.

In addition to the numerous faults, we observed many steeply dipping fractures that lack any apparent displacement. These features, which are particularly abundant in the south-dipping strata exposed between 7 and 17 m north, are typically irregular in cross section and are generally bounded by brecciated zones 1−25 mm thick. The fractures lack evidence of shearing, and most do not displace stratigraphic markers. They do not exhibit preferential development within more clay-rich horizons, indicating that they are not clay shrinkage cracks. On the basis of the absence of shearing and significant stratigraphic displacements on the many fractures observed in the trenches, we interpret these features as cracks associated with seismic shaking and/or bending deformation associated with folding events.

Structural and stratigraphic observations indicate that at least three, and probably four main fault zones are exposed in the trench. From north to south, these are faults 1 through 4 (Fig. 6).

Fault 1

Fault 1 encompasses a 3-m-wide zone of more than 12, closely spaced faults between 42.2 and 45.5 m north (Fig. 8). All of these faults dip steeply south and have normal, south-side-down separations that range from a few millimeters to 25 cm. Most faults have 3–15 cm of dip separation. Cumulative south-side-down separation is ~70 cm. Many strands also show evidence for strike-slip offset in the form of truncated beds and mismatches in bed thickness across individual fault strands (e.g., fault at 42.5 m north, 4.2 m depth). These observations require a component of strike-slip motion, and indicate oblique-normal displacement across fault 1. All of the fault 1 strands terminate at the same stratigraphic level within a 60–100-cm-thick massive silt bed at 1.5–2.5 m depth.

Fault 2

At 34.5 m north the near-vertical main strand of fault 2 juxtaposes the 2-m-thick gravel bed at the south end of package IV with the massive clayey silt deposit of package III (Fig. 8). Total north-side-up vertical separation of the gravel bed across this strand is ≥1.9 m. The bounding fault cannot be traced upward into the massive clayey silt. Possible buried ground surfaces within the clayey silt suggest a complex depositional history, an inference supported by a small, granule-rich sand deposit at 3.7 m depth along the southern, fault-bounded edge of the gravel (thin black triangular-shaped bed extending southward from main package III gravel bed into the massive clayey silt in Fig. 8). The sand layer appears to have been displaced ~10–15 cm down to the south from a similar wedge-shaped bed that extends 35 cm northward into the gravel bed. Alternatively, the sand wedge within the silt deposit may have been displaced ~35 cm down to the south from a silty sand bed near the top of the main gravel bed. Between 37.5 and 43 m north the top of the gravel is nearly horizontal; to the south, the top of the gravel and the parallel sandy silt bed gradually roll over into a 40°S dip toward fault 2, suggesting that the southern part of the gravel has been drag folded down to the south.

A few tens of centimeters north of the main strand of fault 2, a second major strand extends entirely through the gravel (Fig. 8). This steeply south dipping fault is defined within the gravel by a 3–8-cm-wide, planar zone of aligned pebbles. At the top of the gravel bed at 36.3 m north, the northern strand of fault 2 truncates the 5-cm-thick sandy silt bed at the top of the gravel and displaces the contact between the gravel and the overlying massive silt ~10 cm down to the south. We could not trace the fault upward into the silt.

Fault 3

Fault 3 encompasses a zone of steep, north-dipping faults between 22 and 24 m north. Collectively these faults appear to be associated with tilting of the thick gravel bed exposed from 22 to 30 m north. At the base of the trench, fault 3 exhibits a single predominant gouge zone 3–10 cm wide with several thinner splays subparallel to the main strand in an anastomosing zone ~5–20 cm wide. The fault 3 gouge zone is much thicker and better developed than that of any other fault in the trench. In the trench floor the main fault strand is oriented N76E, 74N. The anastomosing fault zone widens upward, reaching >120 cm width at 3.2 m depth. At this depth individual fault strands range in orientation from N75E, 40N to N84W, 88S.

Trench T-2 reveals that fault 3 splays westward into three different strands; a north-dipping southern strand, a near-vertical central strand, and a steep, south-dipping northern strand (Fig. 6). The two northern strands exhibit south-side-up separation, whereas the southern strand exhibits north-side-up separation. Taken together, the fault 3 strands in trench T-2 define a crude, positive flower structure.

In trench T-1 the wide fault zone and the friable deposits within it have been extensively burrowed by gophers and ground squirrels, resulting in a nearly massive deposit above 3.2 m depth, through which the fault cannot be traced on the basis of textural evidence. However, a very sharp, steeply dipping color contrast within the silt unit below the tabular gravel body projects updip from 2.4 m depth at 23 m north to 1.8 m depth at 22 m north. We interpret this planar feature as the updip continuation of the main fault plane. We could not trace the fault up into the argillic horizon of paleosol 2.

The south-dipping gravel wedge (unit 2Bt1) that forms the northern third of the paleosol 2 argillic horizon exhibits an abrupt, 40° angular discordance within <1 m lateral distance with the lithologically identical, north-dipping gravel bed at 21.5 m north (Fig. 7). This geometric relationship cannot be depositional, and we interpret the south-dipping gravel unit as a colluvial wedge composed of material that was eroded from the north-dipping gravel bed and transported downslope. If this inference is correct, then fault 3 must project through the lower part of paleosol 2 at about 21.5 m north, directly updip from the sharp color contrast at 1.8–2.4 m depth. Although in this interpretation the most recent surface rupture along fault 3 extended upward along the southern edge of the north-tilted gravel bed to <1 m depth, the shallowest part of the fault between ~1 and 1.4 m depth would have been obliterated during the postevent scarp collapse that resulted in deposition of the 2Bt1 colluvial wedge.

The silt bed that underlies the gravel colluvial wedge (2BC1 and 2Bt3 in Fig. 7) also exhibits a southward-thinning, wedge-shaped geometry. On the basis of this geometric similarity to the 2Bt1 wedge, and the northern, faulted termination of the 2BC1 deposit, we interpret the silt bed as a colluvial wedge that was deposited during erosion of the silt and granule beds now exposed north of fault 3 and beneath the north-tilted gravel bed from 23.5

to 25.2 m north. The absence within the silt wedge of common Santa Monica Slate clasts greater than granule size indicates that the north-dipping gravel bed was not exposed at the surface at the site of the trench until after the silt wedge was deposited.

Fault 4

Major stratigraphic differences across the unexposed, 1.5–2-m-wide electrical conduit zone at 16.5–18.5 m north reveal the presence of a probable fault (fault 4) (Fig. 7). Vertical separation across the electrical conduit zone (i.e., postulated location of fault 4) is consistently north side up, but the amount of separation varies widely, even between the tops and bases of individual beds. For example, the maximum vertical separation of 115 cm occurs on the top of a gravel bed exposed from 3 to 4 m depth (plus symbols in Fig. 7). In contrast, the separation across the base of the bed is only about 30 cm. This difference is partly a function of the different thicknesses of the bed on either side of the fault, 110 cm to the north versus only 35 cm to the south. Although several beds (e.g., 3A in Fig. 7) exhibit no apparent vertical separation, contacts above and below are vertically separated more than would be expected based solely on their dips projected across the unexposed interval.

Although it is possible that the unexposed interval does not conceal a fault, in this case the stratigraphic differences across the interval would have to reflect strata with exceptionally variable thicknesses across the unexposed interval. We consider this possibility to be unlikely, given the absence of such stratal thickness variations elsewhere in package II, with the local exception of strata deformed by fault 3. These observations are most consistent with the existence of a steeply dipping fault with a significant strike-slip component of movement. The dip of the probable fault is between 55°N and 65°S. In Figure 7 we portray fault 4 with a steep northward dip, consistent with the dips of nearby faults and fractures. Unit 2A, which north of 7 m north exhibits little lateral variation in thickness, abruptly changes in thickness across the postulated fault. Channelization of the 2A horizon appears to be an unlikely explanation of this geometry, because both the top and base of the underlying gravel bed (unit 2Bt1) are displaced by the same amount. The change in 2A thickness may represent strike-slip juxtaposition of parts of 2A of differing thickness, or the change in thickness may record development of a small colluvial wedge on the downslope (south) side of fault 4 after the most recent surface rupture.

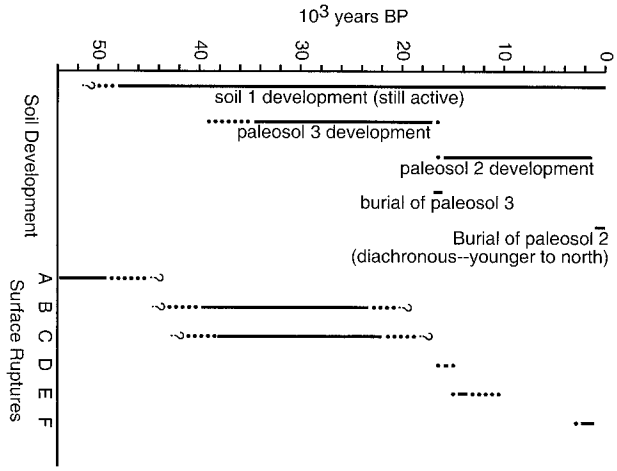

Figure 9. Summary of age estimates for soil development and paleosurface ruptures.

The thickness of the paleosol 2 argillic horizon (units 2Bt1 and 2Bt2) is also different on either side of the unexposed interval. To the south of the unexposed interval, the argillic horizon is lithologically controlled, being restricted to the 25–35-cm-thick gravelly silt bed that extends southward from the gravel wedge. North of the conduit, the argillic horizon is 65–80 cm thick, and has developed completely through the gravel wedge (2Bt1) and into the upper part of the underlying silt bed (2Bt3 in Fig. 6).

Ages of Paleoearthquakes on the Santa Monica Fault

The lack of tilting of the late Holocene Sepulveda fan strata, coupled with the upward termination of all fractures and faults observed in the trenches either at or below the paleosol 2A horizon, indicates that the most recent earthquake on the Santa Monica fault occurred before deposition of the oldest exposed flat-lying strata, probably ca. 1 ka. Trench T-1 contains evidence of at least six ancient surface ruptures. These six paleoearthquakes are discussed here as, from oldest to youngest, events A through F. In general, the stratigraphic and structural relations are better represented for the more recent events.

Event A

The earliest surface rupture is revealed by the south-side-down, oblique-normal displacements across fault 1. The silt bed within which all fault 1 strands terminate is overlain by an unfaulted gravel bed (circled A in Fig. 8). Because the argillic horizon of well-developed surface soil 1 has accumulated down through the unfaulted gravel, deposition of the gravel, which occurred after event A, must predate soil 1 development. We estimate that soil 1 development required ~50 k.y. (Table A1; Figures A1 and A2). Thus, event A is at least this old (Fig. 9). We note, however, that large error bars are associated with the soil age estimate, and the true age of this event may be as young as a few tens of thousands of years. The absence of any well-developed soils between the surface soil and the event horizon suggests that event A occurred within a few thousand years of the onset of soil 1 development. Although most strands of fault 1 appear to terminate at the same stratigraphic level, we cannot be certain that these record only one event.

Events B and C

The 1.8-m-thick gravel bed at the south end of package III has at least 1.9 m of vertical separation across the southern strand of fault 2 (circled B in Fig. 8), whereas the overlying clayey silt bed has only ~10–15 cm of separation across the granule-rich sand wedge at 3.7 m depth (circled C in Fig. 8). These observations indicate that fault 2 has undergone at least two events, which we refer to as events B (older) and C (younger). The lack of cross-fault correlations between the gravel bed and the massive clayey silt precludes determination of whether the southern strand of fault 2 has undergone more than the minimum two events that we identify. Furthermore, displacements on both of the two main fault 2 strands extend up through the top of the gravel bed into the overlying clayey silt. Because of the massive nature of the silt, the upward terminations of these two strands could not be determined. Consequently, it is unclear whether the two strands terminate at two different

stratigraphic levels, and we cannot say whether the two strands record the same earthquake, or two separate events.

In any case, both strands extend much higher in the section than do the fault 1 strands that slipped during event A. Events B and C (and any other earthquakes that occurred on fault 2 during this interval), therefore, occurred after event A. North of ~55 m north the upper part of the massive clayey silt and associated deposits to the north interfinger with the main package IV gravel body (exposed from 53.5–100 m north), through which soil 1 developed over several tens of thousands of years (Fig. 6). Events B and C therefore must have occurred during soil 1 development, well before event D (Fig. 9).

Event D

Event D is recorded by the lower silt colluvial wedge in package II. We infer that this colluvial wedge formed during erosion of a scarp formed during the event. The absence of gravel within the wedge indicates that only silt was exposed at the time of wedge deposition; the distinctive Santa Monica Slate–rich pebble gravel was not yet exposed at the surface. This relationship requires exposure of the tilted gravel bed through either continued, postevent D uplift or lateral motion along fault 3. The event D wedge directly overlies the buried A horizon of paleosol 3, and development of the wedge probably occurred soon after burial of paleosol 3 ca. 16–17 ka. This inference is supported by the position of the event D colluvial wedge in the lowest part (BC horizon) of paleosol 2. The wedge must therefore predate virtually all paleosol 2 development. The SDI and MHI analyses of paleosol 2 indicate that it required ~15–19 k.y. to develop (Table A1; Figures A1 and A2). This suggests that paleosol 2 development began within at most a few thousand years after burial of paleosol 3 (Fig. 9). This, in turn, indicates that the beds through which paleosol 2 developed, including the event D silt colluvial wedge, were deposited very rapidly after burial of paleosol 3.

Event E

Event E is recorded by the 2Bt1 colluvial wedge, as well as by the numerous fractures that terminate at, and just below, the base of the paleosol 2 argillic horizon (these are particularly prominent in trench T-2). Deposition of the southward-fining wedge marks the first appearance of abundant, gravel-derived colluvium in the south-tilted sequence. Because the paleosol 2 argillic horizon is developed through the event E colluvial wedge, the ~1 k.y. burial age of paleosol 2 represents the absolute minimum age for this earthquake. The colluvial wedge forms an integral part of the paleosol 2 profile, however, and therefore predates most paleosol 2 pedogenesis. Paleosol 2 required ~15–20 k.y. to develop (Table A1; Figures A1 and A2), which suggests that event E probably occurred well before ca. 10 ka (Fig. 9). Event E must postdate the burial of paleosol 3 ca. 16–17 ka.

Event F

Direct evidence for this possible earthquake is obscured by the electrical conduit at 16.5–18.5 m north. However, the marked thickness changes of strata on either side of the unexposed interval are most readily explained by the presence of a fault. These lateral thickness changes are most pronounced below the buried A horizon of paleosol 3 (unit 3A). Stratigraphic anomalies, however, suggest that the fault extends to the A horizon of paleosol 2, where fault 4 appears to displace the base of the paleosol 2A horizon ~30 cm down to the south. The upper surface of the paleosol 2 A horizon is not displaced, indicating that if the apparent displacement records a paleo-earthquake, then the surface rupture must have occurred during deposition of unit 2A. Downslope thinning of unit 2A between 14 and 16.5 m north suggests that a small colluvial wedge may have developed after the most recent fault 4 surface rupture.

The paleosol 2 argillic horizon (units 2Bt1, 2Bt2, and 2Bt3) appears to be displaced by fault 4. Thus, event F must have occurred after event E. Furthermore, because the downdropped argillic horizon on the south side of the fault has not thickened to match the thickness of the argillic horizon to the north, event F must have occurred after all but ~1–2 k.y. of paleosol 2 development. The complete absence of deformation in the overlying Sepulveda fan strata indicates that event F must have occurred at least ca. 1 ka. Thus, if these stratigraphic complexities record an earthquake, event F probably occurred between about 1 k.y. and 2–3 k.y. ago (Fig. 9). We emphasize, however, that these stratigraphic relations may not record a surface rupture, although we consider this the most likely explanation.

In summary, there is evidence of variable quality from the trenches for at least 6 paleosurface ruptures during the past ~50 k.y. (Fig. 9). The age estimates for the older events on faults 1 and 2 are based on our poorly constrained estimate of the duration of soil 1 development north of ~25 m north, whereas our age estimates for the fault 3 and 4 events are based on independent, better constrained bulk-soil and detrital charcoal ages. Some older events may be missing from the stratigraphic record. For example, if the silt layer that defines the event horizon for event A actually represents two distinct sediment pulses, separated by a stratigraphically unrecognized hiatus, then more than one event may have occurred on fault 1. Similarly, the two main strands of fault 2 may have moved at different times. In addition, the southernmost strand of fault 2 may have undergone more than the two paleo-earthquakes that we identified. The anomalously well-developed nature of the fault 3 gouge zone, coupled with the extreme deformation associated with the north-tilted gravel unit, strongly suggests that this near-vertical fault has undergone multiple earthquakes, possibly more than the two we identified. We note, however, that the stratigraphic relations indicate that any missing events on fault 3 probably occurred before burial of paleosol 3. Additional events may have occurred south of the trenches beneath Ohio Avenue; although T-1 extended 20 m south of the topographic scarp, the scarp is partly buried at the trench site by recent Sepulveda fan alluvium, and active deformation may extend to the south of the trench. High-resolution seismic reflection data collected across the trench site, however, indicate that the thrust-fault strand of the fault system projects to the projected surface of south-dipping package II within 10 m of the south end of the trench, suggesting that we may have excavated all active surficial strands of the fault zone (Dolan and Pratt, 1997; Pratt et al., 1998).

Because of the possibility of missing older events, we restrict our discussion of recurrence intervals on the Santa Monica fault to the three events that we interpret to have occurred on faults 3 and 4 since burial of paleosol 3 ca. 16–17 ka. The occurrence of these three events between ca. 16–17 ka and 1–3 ka indicate an average latest Pleistocene–Holocene recurrence interval of ~7−8 k.y. for Santa Monica fault earthquakes large enough to cause surface rupture. Although we do not use the pre-17 ka events in the following calculations, we note that the occurrence of six total events during the past ~50 k.y. yields a maximum average recurrence interval for large events of ~10 k.y. This value is similar to the latest Pleistocene–Holocene average recurrence interval, suggesting that relatively few events may be missing from the older part of the record.

We consider it highly unlikely that earth-

quakes large enough to produce surface ruptures would not also rupture the shallow thrust part of the Santa Monica fault beneath the trench (Dolan and Pratt, 1997; Pratt et al., 1998). Events A through F appear to record a southward progression of active surface faulting on faults 1 through 4. We interpret this southward progression as a result of southward propagation of the shallow thrust fault during aggradation of the Sepulveda fan to the south. Thus, the south-tilted package II strata were tilted most recently during displacement on the shallow thrust fault during event F. The onlapping flat-lying strata have not yet undergone an earthquake, but will probably be tilted in a future event associated with surface rupture occurring either on fault 4 or a younger fault south of fault 4.

DISCUSSION

Kinematics of the Santa Monica Fault

Evidence for a consistent component of north-side-up, reverse motion on the Santa Monica fault includes south-facing scarps, south-tilted strata beneath the scarps, vertical separation of the stage 5e marine terrace at Potrero Canyon, and active alluvial fan deposition south of the fault scarp. Despite the absence of left-laterally offset geomorphic indicators (e.g., offset drainages), there is also abundant evidence for a component of left-lateral strike-slip motion along the Santa Monica fault. The numerous strike-slip faults observed in the trenches require strike-slip offsets along the fault zone. In addition, one of the most striking features of the onshore part of the fault is the left-stepping, en echelon pattern of faulting. Because the trench data show that the scarps are contractile structures—best described as fold scarps, rather than true fault scarps—the left-stepping pattern indicates that the scarps developed in response to a left-lateral shear couple. Evidence for both a contractional component of deformation on the thrust fault beneath the trench (Dolan and Pratt, 1997; Pratt et al., 1998) and left-lateral strike-slip motion on the steeply dipping faults in our trench indicates near-surface strain partitioning along a fault that exhibits oblique, reverse, and/or left-lateral motion at depth.

Relationship of the Santa Monica Fault to the Hollywood, Malibu Coast, Anacapa-Dume, and Santa Cruz Island Faults

Both the Santa Monica and Hollywood faults are north-dipping faults that exhibit components of both reverse and left-lateral strike-slip motion (Dolan and Sieh, 1992; Dolan et al., 1995, 1997; this study). Coupled with the similar orientations of the two faults, their similar kinematics lead us to interpret them as closely related strands within a single fault system that might potentially rupture together during large earthquakes (Fig. 2). Oblique left-lateral slip on these faults indicates that the 1.2 km left step at the west Beverly Hills lineament is a releasing bend, which could potentially act as an earthquake segment boundary (Sibson, 1985). The relatively narrow width of this stepover, however, suggests that it may not be an effective barrier to dynamic rupture propagation across the step (Harris and Day, 1993, 1998). Subsurface data indicate a generally gentler near-surface dip (~30°–35°) for the Santa Monica fault in the upper few hundred meters than for the Hollywood fault (Wright, 1991; Dolan and Pratt, 1997; Dolan et al., 1997; Pratt et al., 1998; Tsutsumi at al., 2000). Thus, the left step at the Santa Monica–Hollywood fault intersection may simply reflect differing near-surface dips, and the west Beverly Hills lineament may be a tear fault. The dip of the Santa Monica fault, however, steepens downdip, and the two faults may merge into a single structure at seismogenic depths.

In contrast to the relatively simple Santa Monica–Hollywood fault connection, the kinematics of fault interactions at the west end of the Santa Monica fault are not well determined. Because the Santa Monica fault constitutes the central section of the >200-km-long, oblique-reverse and left-lateral Transverse Ranges Southern Boundary fault system, left-lateral strike-slip motion carried by the Santa Monica fault is apparently transferred westward to the left-lateral Santa Cruz Island and Santa Rosa Island strike-slip faults, at the west end of the system. The most obvious candidate fault for this transfer is the Malibu Coast fault, a left-lateral strike-slip fault that extends 55 km along the Malibu coast (Figs. 1 and 3; Dibblee, 1982; Drumm, 1992; Treiman, 1994). The Malibu Coast fault trends offshore to the east of Malibu and may merge eastward with the Santa Monica fault; in the past the offshore part of the Santa Monica fault has sometimes been referred to as the Malibu Coast fault (e.g., Vedder et al., 1986). At its western end 15 km south-southwest of Port Hueneme, the Malibu Coast fault appears to connect with the left-lateral Santa Cruz Island fault to the southwest through an 8-km-wide left step (Fig. 1; Sorlien, 1994). These relations suggest that the Malibu Coast fault has acted to transfer left-lateral strike-slip westward from the Santa Monica fault onto the Santa Cruz Island fault. Recent geomorphologic results, however, raise the possibility that the Malibu Coast fault may be much less active than in the past, and may no longer be active. Treiman (1994) suggested that the strike-slip rate on the fault has been diminishing throughout Pleistocene time, and that the current rate appears to be $\ll$0.5 mm/yr. If left-lateral motion along the southern boundary of the Transverse Ranges to the west of Point Dume is not carried along the Malibu Coast fault, then some other fault(s) must serve to connect the Santa Monica and Santa Cruz Island faults.

The other major fault in the region is the moderately north dipping Anacapa-Dume fault, which extends 40 km from ~7 km southeast of Point Dume westward to a point due south of Port Hueneme, where it terminates in the complex zone of faulting at the stepover between the Malibu Coast and Santa Cruz Island faults (Fig. 1) (Junger and Wagner, 1977; Vedder et al., 1986; Sorlien, 1994). The 1973 M_w 5.3 Point Mugu earthquake, the largest event to occur in the Malibu coast region during the instrumental period, probably occurred on the Anacapa-Dume fault (Stierman and Ellsworth, 1976; Hauksson, 1990; Bent and Helmberger, 1991; Treiman, 1994). The focal mechanism of the main shock reveals oblique motion, with nearly equal amounts of left-lateral and reverse slip (strike slip [ss]:reverse slip [rev] 0.7:1); aftershocks and subsequent small earthquakes exhibit a mixture of reverse and oblique reverse-left-lateral focal mechanisms (Stierman and Ellsworth, 1976). These seismicity data suggest that the oblique-slip Anacapa-Dume fault accommodates a significant component of left-lateral motion.

Left-lateral motion may be transferred between the Santa Monica and Santa Cruz Island faults in several possible ways: (1) the Malibu Coast fault may not be inactive (or nearly inactive), as proposed by Treiman (1994), and still serves to transfer left-lateral motion; (2) some as-yet unidentified strike-slip fault exists north of the Anacapa-Dume fault along the shelf; or (3) oblique slip on the Anacapa-Dume fault may serve to transfer the left-lateral strike-slip motion, but that left-lateral component of motion is diluted by a slightly more rapid component of reverse slip than occurs on either the Santa Cruz Island or Santa Monica faults. We speculate that the Anacapa-Dume fault may represent part of the frontal fault system that accommodates a higher degree of the convergence across the Transverse Ranges than do the Santa Monica or Santa

Cruz Island faults, where much of the contractional deformation may be accommodated along blind thrust faults (Davis et al., 1989; Shaw and Suppe, 1994, 1996; Dolan et al., 1995). The northwest-striking, right-lateral Palos Verdes fault, which to the south is slipping at ~3 mm/yr (Ward and Valensise, 1994; Stephenson et al., 1995; McNeilan et al., 1996), terminates against the frontal fault system at the eastern end of the Anacapa-Dume fault (Fig. 1). This relationship suggests that the Anacapa-Dume fault may have developed at least partially in response to more rapid north-south shortening west of the Palos Verdes fault.

Relationship to Santa Monica Mountains Blind Thrust Fault

Davis et al. (1989) and Davis and Namson (1994) postulated that the Santa Monica Mountains are the surface expression of a fault-propagation fold that has developed in response to motion on a gently north-dipping, blind thrust fault, which we refer to as the Santa Monica Mountains thrust fault (Dolan et al., 1995; western part of the Elysian Park thrust system of Davis et al., 1989). Davis and Namson (1994) inferred that fault activity began ca. 2.5–3 Ma and suggested an average slip rate for this interval of 3.8–5.9 mm/yr. Their model shows the Santa Monica fault as a steep, north-dipping, structurally inverted, normal fault that intersects the blind thrust fault at ~15 km depth. Several lines of evidence, however, call into question the high average slip rate proposed by Davis and Namson (1994).

1. Active alluvial fan deposition along the southern flank of the Santa Monica fault scarp, 3–4 km south of the topographic mountain front, suggests that uplift is currently concentrated at the surface fault trace. The occurrence of active uplift well to the south of the mountain front is supported by the presence of older, dissected, and segmented alluvial surfaces between the fault scarp and the mountain front. These older fan segments imply that the mountain front is not actively being uplifted, as would be expected if the mountains were an actively growing anticline, the forelimb of which intersected the onlapping alluvial deposits at the topographic mountain front.

2. Seismic reflection profiles show that for several kilometers south of the Santa Monica fault Pleistocene to Holocene strata are flat lying. The flat-lying nature of these strata indicates that no folding or tilting has occurred in this region for at least several hundred thousand years (Wright, 1991; Dolan and Pratt, 1997; Pratt et al., 1998; Tsutsumi et al., 2000). The lack of significant deformation appears to be at odds with the position of these strata in the forelimb of a fault-propagation fold above a rapidly slipping blind thrust fault.

3. The slow (~0.1–0.2 mm/yr) regional uplift rate of the ca. 120 ka marine terrace at Point Dume and Pacific Palisades (excluding near-field uplift related to the Santa Monica fault) appears to be incompatible with the high (3.8–5.9 mm/yr) slip rates on the blind thrust proposed by Davis and Namson (1994). Furthermore, in Pacific Palisades the ca. 120 ka marine terrace is above the forelimb of the Santa Monica Mountains anticlinorium. Although a structure contour map of the terrace based on borehole data indicates local dips that may be as steep as 14° (McGill, 1989), regionally the abrasion platform tilts seaward at ~1°. This observation suggests that the terrace has not been significantly tilted, as might be expected if the Davis and Namson model is correct.

Collectively, these observations indicate that the Santa Monica Mountains blind thrust fault must be slipping at a rate far slower than the 3.8–5.9 mm/yr rate proposed by Davis and Namson (1994). In the extreme case, the fault may no longer be active. In either case the blind thrust fault appears to represent less of a seismic hazard than has been proposed (e.g., Davis et al., 1989; Davis and Namson, 1994; Dolan et al., 1995).

Another possibility is that the surficial Santa Monica fault and the postulated blind thrust could be the same fault, possibly as a result of propagation of the Santa Monica fault up through the forelimb of the Santa Monica Mountains fold during Pleistocene time. If so, then the 0.6 mm/yr dip-slip rate on the Santa Monica fault would translate into a north-south shortening rate of ~0.4 mm/yr, an order of magnitude slower than the 3.5–5.4 mm/yr north-south shortening rate implied by the Davis and Namson model. The very slow (0.1–0.2 mm/yr) uplift rate of the coast south of the Santa Monica fault, however, implies the presence of an active fault, albeit one with a slow slip rate, beneath the Santa Monica fault.

Limits on the Slip Rate of the Santa Monica Fault

The ~0.6 mm/yr reverse slip rate determined at Potrero Canyon provides a minimum overall slip rate for the Santa Monica fault. This is only a partial slip rate, however, because it does not take into account any left-lateral slip. Dense urbanization prevented us from excavating a three-dimensional trench network designed to assess the strike-slip rate and the ratio of strike-slip to dip-slip motion. Because no laterally offset piercing points are available, left-lateral offsets on individual faults exposed in the trench cannot be determined. However, the extreme deformation observed along near-vertical strike-slip faults in the trenches (e.g., truncation of 2-m-thick gravel by fault 2, northward tilting of gravel by fault 3) implies that at least some of the major faults have significant displacements. Furthermore, although slip on each of the numerous lesser faults may be small (millimeters to meters?), the large number of these faults indicates that cumulative strike slip across the entire fault zone may be large. We suspect that the actual strike-slip rate on the Santa Monica fault may be relatively fast; in the western part of the Transverse Ranges Southern Boundary fault system left-lateral strike-slip rates on the Santa Rosa Island and Santa Cruz Island faults are ~1 mm/yr and 0.75 mm/yr, respectively (Colson et al., 1995; Pinter et al., 1995). The oblique-slip rate for the Santa Monica fault could therefore potentially be as fast or even faster than the dip-slip rate. Nevertheless, in the absence of a measured ss:rev ratio, in the following discussion we conservatively use only the 0.6 mm/yr dip-slip minimum rate.

Size and Frequency of Future Santa Monica Fault Earthquakes

One of the most important questions facing seismic hazard planners in metropolitan Los Angeles concerns the size of future earthquakes. For example, does the Santa Monica fault typically rupture in moderate events similar in size to the 1994 Northridge M_w 6.7 event? Or does the fault break during much larger ($M_w \geq 7.0$), but less frequent earthquakes? One means of answering these questions is to use fault-plane areas and slip rates to estimate the sizes and recurrence intervals for hypothetical earthquakes, and then to compare those calculated values with measured recurrence intervals. For example, regressions of moment-magnitude versus rupture area and average displacement indicate that rupture of the entire 40-km-length of the Santa Monica fault could produce a M_w ~6.9–7.0 earthquake, with an average displacement of ~1.1–2.0 m (Wells and Coppersmith, 1994; Dolan et al., 1995). The minimum, 0.6 mm/yr reverse-slip-only rate for the fault indicates a maximum recurrence interval for such events of ≤~1.9–3.3 k.y. We emphasize, however, that use of a higher slip rate in this calculation results in a commensurately shorter calculated

average recurrence interval. For example, an arbitrary slip rate of 1 mm/yr yields an average recurrence interval for M_w 6.9–7.0 events of ~1.1–2 k.y.

The ~7–8 k.y. latest Pleistocene–Holocene average recurrence interval that we determined for Santa Monica fault surface ruptures is considerably longer than the calculated intervals for M_w 6.9–7.0 earthquakes involving rupture of the entire fault. This marked disparity suggests either that: (1) many events are missing from the post-17 ka trench record, a possibility that we think is unlikely given that there is evidence for only one potential surface rupture that deforms the strata through which paleosol 2 has developed; or (2) the Santa Monica fault undergoes very infrequent, and therefore large ($M_w \geq 7.0$) earthquakes, possibly larger than those that would result from rupture of the entire Santa Monica fault. We speculate that if such events have occurred, they have involved simultaneous rupture of the Santa Monica fault together with adjacent faults in the Transverse Ranges Boundary fault system (e.g., the Hollywood fault and Anacapa-Dume faults).

Implications for Seismic Hazard Assessment in Metropolitan Los Angeles Basin

The Santa Monica fault appears to be capable of generating earthquakes as large as M_w 6.9–7.0, considerably larger than the M_w 6.7 1994 Northridge event, which directly caused 31 deaths and resulted in more than $40 billion in damage (Scientists of the USGS/SCEC, 1994). As discussed herein, the apparently long recurrence intervals for the Santa Monica fault are most consistent with rupture of the fault in large ($M_w \geq 7.0$), infrequent earthquakes possibly involving rupture of multiple faults in the Transverse Ranges Southern Boundary fault system. The effects of such large earthquakes would be dramatically different from the Northridge event, producing strong ground shaking over a much wider area with a longer duration.

The location and style of faulting on the Santa Monica fault further compound the problems presented by such large earthquakes. The Northridge earthquake occurred beneath the San Fernando Valley, a predominantly residential region northwest of the Los Angeles basin. In contrast, the eastern part of the Santa Monica fault traverses a much more densely urbanized area. Furthermore, unlike the blind thrust fault that produced the Northridge earthquake, the trench data indicate that the Santa Monica fault ruptures to the surface in large earthquakes. In addition to the obvious implications for infrastructure damage associated with potentially large surface displacements, surface-rupturing earthquakes are likely to excite much stronger long-period surface waves than the Northridge event (e.g., Liu and Heaton, 1984; Vidale and Helmberger, 1988; Olsen and Archuleta, 1996). Such long-period surface waves could represent a significant hazard to the many high-rise buildings in the region (Heaton et al., 1995; Olsen and Archuleta, 1996).

Source directivity during future Santa Monica fault earthquakes could also play a critical role in determining damage patterns. If, for example, a hypothetical earthquake were to nucleate near the eastern end of the fault and propagate westward, damage might be centered in the Westwood–Santa Monica–Malibu region, but much of the energy would be dissipated beneath the Pacific Ocean and the sparsely populated western Santa Monica Mountains. However, if hypothetical rupture were to start at the western end of the system and propagate eastward, older, vulnerable structures in the Hollywood, downtown Los Angeles, and east Los Angeles regions would undergo high accelerations and velocities. These parts of the city were among the first to be urbanized, and they contain some of the region's most vulnerable, and most densely occupied buildings. In addition to older structures, the latter scenario would focus energy toward the high-rise corridor that extends east-west from downtown Los Angeles to Santa Monica. The stability of some of these structures during relatively close, large earthquakes has been the subject of intense scientific discussion (Heaton et al., 1995).

CONCLUSIONS

The Santa Monica fault accommodates oblique, left-lateral-reverse motion, which is partitioned in the near surface at our trench site onto a wide zone of closely spaced strike-slip faults exposed in the trench and a thrust strand beneath trench depth. Paleoseismologic and geomorphologic data indicate that the fault is active and capable of producing damaging earthquakes beneath the densely urbanized northwestern corner of the Los Angeles area and offshore along the Malibu coast. The measured ~7–8 k.y. latest Pleistocene–Holocene average recurrence interval for surface ruptures is considerably longer than the recurrence interval calculated for a hypothetical M_w 6.9–7.0 earthquake generated by rupture of the entire Santa Monica fault. Unless many events are missing from the post-17 ka trench record—a possibility that we think is unlikely—this disparity implies that the Santa Monica fault has undergone infrequent, and therefore very large ($M_w \geq 7.0$), earthquakes, possibly larger than those associated with rupture of the entire Santa Monica fault. We speculate that such large events may involve simultaneous rupture of the Santa Monica fault together with other faults in the Transverse Ranges Southern Boundary fault system, such as the adjacent Hollywood and Anacapa-Dume faults. The occurrence of such large earthquakes beneath the densely populated northwestern Los Angeles basin could produce enormous damage and must be considered in future planning scenarios for the Los Angeles metropolitan region.

APPENDIX

Soil descriptions and age determinations (Table A1) use SDI (soil development index) and MHI (maximum horizon index) methods. Regression method is from Rockwell et al. (1990). Sample localities are shown in Figures 5 and 6. Soil profile SMFT1a (unit 2) is from paleosol 2 at 7.5 m north (SP1 in Fig. 6); soil profile SMFT1a (unit 3) is from paleosol 3 at 7.5 m north (SP2 in Fig. 6); soil profile SMFT1b (unit 2) is from paleosol 2 at 10 m north; soil profile SMFT1b (unit 3) is from paleosol 3 at 10 m north; soil profile SMFT-1c is from 20.8 m north; soil profile SMFT4a is from surficial soil 1 at 97.5 m north (SP4A in Fig. 5); soil profile SMFT4b is from surficial soil 1 at 79.7 m north (SP4B in Fig. 5).

ACKNOWLEDGMENTS

We thank Donovan Stevens, Sally McGill, Judy Zachariasen, Jim Spotila, Richie Wolf, Danny Schambach, and Michael Slates for help with trench work. We are indebted to Dick Crook and Scott Lindvall for helpful discussions. We also thank the U.S. Veteran's Administration (especially Ben Crockett, Joe Richards, Bill Proper, and Lester Jones) and the American Red Cross (especially Trish Bishoff and Robert Cordero) for allowing us to excavate trenches on their property. This research was funded by grants from the Southern California Earthquake Center (SCEC), the California Department of Transportation, the City of Los Angeles, and the County of Los Angeles. SCEC is supported by National Science Foundation Cooperative Agreement EAR-8920136 and U.S. Geological Survey Cooperative Agreements 14–08–0001-A0899 and 1434-HQ-97AG01718. This is SCEC Contribution 267 and Division of Geological Sciences, California Institute of Technology Contribution 5747.

REFERENCES CITED

Argus, D.F., Heflin, M.B., Donnellan, A., Webb, F.H., Dong, D., Hurst, K.J., Jefferson, D.C., Lyzenga, G.A., Watkins, M., and Zumberge, J.F., 1999, Shortening and thickening of metropolitan Los Angeles measured and inferred using geodesy: Geology, v. 27, p. 703–706.

Barbat, W.F., 1958, The Los Angeles basin area, California, *in* Weeks, L.G., ed., Habitat of oil—A Symposium:

TABLE A1. SOIL DESCRIPTIONS AND AGE DETERMINATIONS

Horizon	Depth (cm)	Thick-ness (cm)	Color	Texture	Structure	Consis-tency	Clay films	Boun-dary	Sand (%)	Silt (%)	Clay (%)	2nd clay (%)	Bulk density	Hi	Sdi	Second. clay vol (gm/cm²)	Notes
Pedon SMFT-1a																	
A/Cn	0–250	250															Late Holocene alluvium
2Ab	250–274	24	10YR3/3m	L	1–2msbk	vfr-fr, ss,ps-p	n.o.	a,w	42.18	42.60	15.22	5.22	1.17			1.47	^{14}C-1 from 2Ab$_1$(buries 2Ab down-slope) may be younger than 2Ab but should be close to burial age
2Bt1b	274–296	22	10YR4/3.5m	CL	3m-cabk	s-vs,p,fr	3n&1mkpf, 3–4nvmkpo, 1nbr, 3–4mkcl	c,s	26.57	42.05	31.38	21.38	1.50		7.04		
2Bt2b/ BC1b	296–317	21	10YR3/4m	SL	1msbk	fr,ss,ps	1npf, 3npo, 2n&1mkbr	c,s	48.51	35.62	15.87	5.87	1.42		1.76		
2BC2b	317–345	28	10YR4/3m	SL	1msbk	fr,ss,ps	vncl, 1npo, vnpf	a,w	49.06	37.52	13.42	3.42	1.52			1.45	Pebbly conglomerate at base of horizon; common Mn stains in pores
														0.58	44.1	**11.72**	Profile totals of HI, SDI, profile mass of secondary clay
														21.3	7.6		Intercept ages (ka)
3Ab	345–368	23	10YR4/3m	SL	2csbk	fr,ss,ps-p	v-1npo	c,w	45.36	43.78	10.86	0.86	1.55			0.31	Common to many Mn stains in pores
3Btb	368–388	20	10YR4/5m	SCL	2cabk	fr-fi,s,p	3–4n-kpf, 4n-mk&2kpo, 1–2nbr, 4kcl	no	42.56	35.14	22.30	12.30	1.54			3.79	Common to many Mn stains on clay films in pores and ped faces
3Btb	388–408	20							44.30	33.25	22.46	12.46	1.64			4.08	
3Btb	408–428	20							40.23	33.14	26.62	16.62	1.59			5.30	
3Btb	428–448	12							44.57	33.12	22.30	12.30	1.58			2.33	
3Btb	448–460+	12							48.49	33.14	18.37	8.37	1.55			1.56	
														0.56	88.1	**17.36**	Profile totals of HI, SDI, profile mass of secondary clay
														19.0	19.4		Intercept ages (ka)
Pedon SMFT-1b																	
L. Hol. Strat Alv.	0–154	154															
2Ab	154–172	18	10YR3/3m, 5/3d		1–2msbk	sh,fr,ss, ps-p		c-a,w	39.33	47.14	13.53	3.53	1.46			0.92	vmvf&mf root pores, few vf and f roots
2Eb	172–178	6	10YR4/3m, 5/3d	SL	1msbk	sh,fr, ss,ps		a,w	41.15	45.07	13.77	3.77	1.29			0.29	Few (ferraus? see M.L.H.) in pores, skeletal leaching
2Btb	178–215	37	10YR4.5/ 4m5/4d	CL	3m-cabk	eh,fi,s-vs,p	4n&1–2mkpf, 4n-mkpo, 1–2nbr	c,s	25.32	43.59	31.09	21.09	1.54			12.04	
2BC1	215–242	27	10YR4.5/3m	L-SL	2csbk	fr,s,p	2n&vmkpf, 2npo	c-g,s	38.87	38.21	22.93	12.93	1.47			5.13	Common v.f. pores, few v.f. roots
2BC2	242–284	42	10YR4.5/ 2.5m	SL	1–2csbk	fr,ss,ps	1npf, 2npo	a,i	44.33	36.94	18.73	8.73	1.50			5.49	
														0.63	55.8	**23.88**	Profile totals of HI, SDI, profile mass of secondary clay
														28.5	9.6		Intercept ages (ka)
Pedon SMFT-1c																	
3AB	0–28	28	10YR5/4d, 10YR4/ 3.5m	L-SL	1–2msbk	fr,ss,ps, sh-h	vnpf	c,w	41.71	42.42	15.87	5.87	1.37			2.25	
3Bt1b	28–48	20	10YR5.5/ 4d,10YR4/ 4m	pebbly CL	2m-cabk	s-vs,p,fi,eh	4n-mkpf, 3–4mkpo, 4n-kcl	c,s	39.87	34.30	25.83	15.83	1.58			5.01	pm = v.f. sand to silty sand with 30% pebbles
3Bt1b	48–68	20							39.37	37.24	23.39	13.39	1.52			4.08	
3Bt1b	68–89	21							37.17	41.17	21.66	11.66	1.54			3.77	
3Bt2b	89–121	32	10YR4.5/ 3m2.5Y–; 10YR5/3d	sgr L	2msbk	s,ps,fr,eh	2–3n&1mkpf, 3mkpo, 3ncl	g,s	33.33	43.94	22.73	12.73	1.55			6.33	
3BC1b	121–146	25	10YR5/3m, 2.5Y5/4d	gr SL-L	1csbk	s-sh,fr-vfr p,ss-s	1–2npf, 2npo&cl	g,s	45.23	36.68	18.08	8.08	1.25			2.53	pm change ~140; Mn staining throughout profile along old root casts
3BC1b	146–172	26							63.69	24.08	12.22	2.22	1.51			0.87	
3BC2b	172–202	30	10YR5/3m, 2.5Y5/4d	sg SL	m-1csbk	vfr,ss,ps, sh	1npf&po, vncl	g,s	67.03	22.41	10.57	0.57	1.42			0.24	
														0.61	86.4	**25.09**	Profile totals of HI, SDI, profile mass of secondary clay
														25.4	18.7		

TABLE A1. (*Continued*)

Horizon	Depth (cm)	Thick-ness (cm)	Color	Texture	Structure	Consis-tency	Clay films	Boun-dary	Sand (%)	Silt (%)	Clay (%)	2nd clay (%)	Bulk density	Hi	Sdi	Second. clay vol (gm/cm²)	Notes
Pedon SMFT 2 (T1b) (N end)																	
A	0–1	1		L	2fcr		n.o.	a,s	38.25	44.05	17.70	9.70	1.41			0.14	
Bt	1–31	30		CL-C	3cabk			c,i	28.60	31.65	39.75	31.75	1.55			14.77	
2Bt	31–62	31		vgCL	2csbk			c,w	34.12	29.16	36.72	28.72	1.60			14.26	
3Bt	62–86	24		CL	3msbk-abk				41.10	30.07	28.83	20.83	1.68			8.39	
3Bt	86–109	23		CL				g,s	42.04	31.07	26.89	18.89	1.74			7.57	
3BC	109–146	37		L-SL	2mabk-sbk			c,w	52.97	27.17	19.85	11.85	1.64			7.21	
3BC	146–183	37		L					50.83	31.45	17.72	9.72	1.63			5.87	
4BC	183–234	51		SL	m - 1 c s b k &sg		a,i		64.70	22.40	12.90	4.90	1.56			3.90	
4BC	234–285	51		SL					76.96	14.37	8.68	0.68	1.73			0.60	
5BC	285–324	39		L	m-2msbk				33.60	43.47	22.94	2.94	1.54			1.77	
5BC	324–363	39		L					37.84	40.99	21.18	1.18	1.57			0.72	
6C	363–390	27		vgSL	m			a,w	57.98	25.03	16.99	16.99	1.59			7.30	
7C	390–430+	40+		L-siL	m-1msbk			n.o.	28.81	49.11	22.09	22.09	1.60			14.11	
																86.61	
Pedon SMFT 4a																	
A	0–14	14	10YR 3/3m, 5/3d	siL	1–2msbk	h, ss, ps	no	c,w	26.93	53.88	19.20		N.D.				
A/B	14–23	9	10YR 3/4m, 4/4d	siCL-CL	2m-csbk	vs, p	n.o.	c,s	22.41	47.15	30.44		N.D.				
Bt1	23–47	24	10YR 3/3m, 4.5/4d	CL	2–3cabk	vs, p	4n,3mk&2kpf, 4n-kpo*	c,s	22.60	42.07	35.33		N.D.				Matrix not plugged
Bt1	47–71	24							26.24	43.40	30.36		N.D.				
Bt2*	71–104	33	2.5Y 4/3m, 5/3d	C	3cabk-pr	s, vp	4kpf&po**	g,s	17.52	37.80	44.68		N.D.				*This may be distinct stratigraphic unit (much finer); **matrix plugged with clay
Bt2*	104–137	33							19.44	39.36	41.20		N.D.				
Bt3	137–166	29	10YR 4/3m, 4/4d	CL	2–3cabk	s, p	3n&2mkpf, 4mk-kpo	a-c,i*	37.98	33.05	28.97		1.54				*Channelized?
Bt3	166–195	29							45.13	29.38	25.49		1.58				
Bt3	195–224	29							51.03	30.52	18.44		1.65				
2BC	224–282	58	10YR 4/4m, 4/4d	vgSL*	m - s g & 1csbk	ss, po	2n&1mkcl**	a,i	76.28	13.47	10.25		1.70				*70% gravel content, ** matrix is mostly clay free
3C	282–320	38	10YR4.5/3m 6/2.5d	sgSL*	m-2csbk	ss, po	1ncl,1copf	a,i	59.14	31.94	8.92		1.51				*~10% gravel
4C	320–380	60	2.5Y 4/3m; 5/2d	vgLS*	m-sg**	so, po	2–3mk-kcl (in clay rich pockets)	a,i	80.91	12.83	6.25		N.D.				*~70% gravel,**except in localized pockets 5%–10% of clay accum.
5C	380–450+	70+	2.5Y 4/3m; 5/3d	LS	m-1csbk	so, po	vcogr		73.84	18.71	7.45		1.49				
														0.71	134.4@ 400 cm		
														45.5	52.0		Intercept ages
Pedon SMFT 4b																	
A	0–4	4	10YR3/2m, 3/3d	L	1–2c cr	h,so,ps	n.o.	c,s	50.36	32.92	16.71	6.71	1.47			0.40	
Bt1	4–38	34	10YR4/2m, 5/3d	SCL	2csbk	h,s,p	4n-kcl&br	g,s	59.19	18.62	22.19	12.19	1.48			5.75	

TABLE A1. (*Continued*)

Horizon	Depth (cm)	Thick-ness (cm)	Color	Texture	Structure	Consis-tency	Clay films	Boun-dary	Sand (%)	Silt (%)	Clay (%)	2nd clay (%)	Bulk density	Hi	Sdi	Second. clay vol (gm/cm^2)	Notes
Bt1	38–73	35		SL-SCL					61.39	18.58	20.03	10.03	1.46			0.73	
Bt1	73–108	35		SL					70.30	11.85	17.86	7.86	1.36			3.75	
Bt2	108–135	27	10YR3/3m, 3/4d	SL	m-1csbk	so,s,p	1–2n-mkcl,2nbr	g,s-w	69.14	16.89	13.97	3.97	1.33			1.43	
Bt2	135–163	28							N.D.	N.D.	N.D.	3.97	1.67			1.86	
BC (lams)	163–197	34	10YR3/3m, 4/4d	SL	m - s g & 1csbk	so,ss,po	3nbr in bands (30%), 1–2ncl,vmkcl		78.03	12.25	9.72	0.00	1.62			0.00	
BC (lams)	197–231	34		SL					76.43	13.15	10.42	0.42	N.D.			0.23	
BC (lams)	231–265	34		SL					76.73	12.10	11.17	1.17	N.D.			0.64	
C	265–290	25	10YR3/2m, 4/3.5d	SL	m - s g & 1csbk	so,so-ss, po	1ncl,vn-mkbr	a,w	74.06	15.83	10.11	0.11	N.D.			0.04	
C	290–315	25							N.D.	N.D.	N.D.	0.11	N.D.			0.04	
2C (mottled)	315–350	35	10YR3/3m, 5/3d	L	m-2csbk	vh,s,p	stains on pf		44.34	35.09	20.57	0.00	1.56			0.00	
														0.58	88.1	**14.88**	Profile totals of HI, SDI, profile mass of secondary clay
														13.4	19.4		Intercept ages (ka)

Notes: Texture: Soil descriptions and age determinations using SDI (soil development index) and MHI (maximum horizon index) methods. Regression method is from Rockwell et al. (1990). Sample localities shown in Figures 6 and 7. Soil profile SMFT1a (unit 2) is from paleosol 2 at 7.5 m north (SP 1 in Fig. 7); soil profile SMFT1a (unit 3) is from paleosol 3 at 7.5 m north (SP 2 in Fig. 7); soil profile SMFT1b (unit 2) is from paleosol 2 at 10 m north; soil profile SMFT1b (unit 3) is from paleosol 3 at 10 m north; soil profile SMFT-1c is from 20.8 m north; soil profile SMFT4a is from surficial soil 1 at 97.5 m north (SP 4A in Fig. 6); soil profile SMFT4b is from surficial soil 1 at 79.7 m north (SP 4B in Fig. 6). S—sand, LS—loamy sand, SL—sandy loam, CL—clay loam, SCL—sandy clay loam, SiL—silt loam, L—loam; Structure: 1—weak, 2—moderate, 3—strong, f—fine, m—medium, c—coarse, sbk—subangular blocky; abk—angular blocky; m—massive, sg-single grain, cr—crumb, pr—prismatic; Dry Consistency: lo—loose, so—soft, sh—slightly hard, h—hard, vh—very hard, eh—extremely hard; Wet Consistency: so—non-sticky, po—non-plastic, ss—slightly sticky, ps—slightly plastic, s—sticky, p—plastic, vs—very sticky, vp—very plastic; Clay Films: v—very few, 1—few, 2—common, 3—many, 4—continuous, n—thin, mk—moderately thick, k—thick, po—pores, pf—ped faces, cl—clast faces, br—grain bridges; Boundary: a—abrupt, c—clear, g—gradual, d—diffuse, s—smooth, w—wavy, i—irregular

American Association of Petroleum Geologists, p. 62–77.

Bent, A.L., and Helmberger, D.V., 1991, Seismic characteristics of earthquakes along the offshore extension of the western Transverse Ranges: Seismological Society of America Bulletin, v. 81, p. 399–422.

Birkeland, P.W., 1972, Late Quaternary eustatic sea-level changes along the Malibu coast, Los Angeles County, California: Journal of Geology, v. 80, p. 432–448.

Bloom, A.L., Broecker, W., Chappell, J.M.A., Matthews, R.K., and Mesolella, K.J., 1974, Quaternary sea level fluctuations on a tectonic coast—New $^{230}Th/^{234}U$ dates from the Huon Peninsula, New Guinea: Quaternary Research, v. 4, p. 185–205.

Chappell, J.M., 1983, A revised sea-level record for the past 300 000 years from Papua, New Guinea: Search, v. 14, p. 99–101.

Colson, K.B., Rockwell, T.K., Thorup, K.M., and Kennedy, G.L., 1995, Neotectonics of the left-lateral Santa Rosa Island fault, western Transverse Ranges, southern California: Geological Society of America Abstracts with Programs, no. 5, v. 27, p. 11.

Converse Consultants Report, 1998, Geologic and seismic hazard investigation, Santa Monica Hospital, Santa Monica, California: Monrovia, California, Converse Consultants Report, Project 98-31-216-01, Converse Consultants, December 21, 1998, v. II, Appendix F, 21 p.

Crook, R., and Proctor, R., 1992, The Hollywood and Santa Monica faults and the southern boundary of the Transverse Ranges province, *in* Pipkin, B., and Proctor, R., eds., Engineering geology practice in southern California: Belmont, California, Star Publishing Company, 1992 p.

Crook, R., Proctor, R., and Lindvall, C.E., 1983, Seismicity of the Santa Monica and Hollywood faults determined by trenching: U.S. Geological Survey Final Technical Report, USGS Contract 14–08–0001–20523, 26 p.

Davis, T.L., and Namson, J.S., 1994, A balanced cross-section of the 1994 Northridge earthquake, southern California: Nature, v. 372, p. 167–169.

Davis, T.L., Namson, J., and Yerkes, R.F., 1989, A cross section of the Los Angeles area: Seismically active fold and thrust belt, the 1987 Whittier Narrows earthquake, and earthquake hazard: Journal of Geophysical Research, v. 94, p. 9644–9664.

Dibblee, T.W., 1982, Geology of the Santa Monica Mountains and Simi Hills, southern California, *in* Fife, D.L., and Minch, J.A., eds., Geology and mineral wealth of the California Transverse Ranges: Santa Ana, California, South Coast Geological Society, p. 7–26.

Dibblee, T.W., 1991, Geologic map of the Beverly Hills and Van Nuys (South 1/2) Quadrangles, Los Angeles County, California: Santa Barbara, California, Dibblee Geological Foundation Map DF-31, scale 1:24 000.

Dibblee, T.W., 1992, Geologic map of the Topanga and Canoga Park (South 1/2) Quadrangles, Los Angeles County: Santa Barbara, California, Dibblee Geological Foundation Map DF-35, scale 1:24 000.

Dibblee, T.W., 1993, Geologic map of the Point Dume Quadrangle, Los Angeles and Ventura Counties: Santa Barbara, California, Dibblee Geological Foundation Map DF-48, scale 1:24 000.

Dolan, J.F., and Pratt, T.L., 1997, High-resolution seismic reflection imaging of the Santa Monica fault zone, west Los Angeles, California: Geophysical Research Letters, v. 24, p. 2051–2054.

Dolan, J.F., and Sieh, K., 1992, Tectonic geomorphology of the northern Los Angeles basin: Seismic hazards and kinematics of young fault movement, *in* Ehlig, P.L., and Steiner, E.A., eds., Engineering geology field trips: Orange County, Santa Monica Mountains, and Malibu, guidebook and volume: Berkeley, California, Association of Engineering Geologists, p. B-20–B-26.

Dolan, J.F., Sieh, K., Rockwell, T.K., Yeats, R.S., Shaw, J., Suppe, J., Huftile, G., and Gath, E., 1995, Prospects for larger or more frequent earthquakes in greater metropolitan Los Angeles, California: Science, v. 267, p. 199–205.

Dolan, J.F., Sieh, K., Rockwell, T.K., Guptill, P., and Miller, G., 1997, Active tectonics, paleoseismology, and seismic hazards of the Hollywood fault, northern Los An-

	SDI	Log Age	95% C.I.		Age	Max	Min
SMFT 1a (Unit 2)	44.1	3.88	4.32	3.44	7,688	20,874	2,767
SMFT 1a (Unit 3)	88.1	4.29	4.76	3.82	19,395	57,432	6,558
SMFT 1b (Unit 2)	55.8	3.98	4.44	3.52	9,585	27,787	3,307
SMFT 1c (Unit 3)	86.4	4.27	4.73	3.81	18,705	54,208	6,455
SMFT 4a	134.4	4.72	5.18	4.25	51,978	158,386	17,975
SMFT 4b	88.1	4.29	4.82	3.76	19,395	65,756	5,721

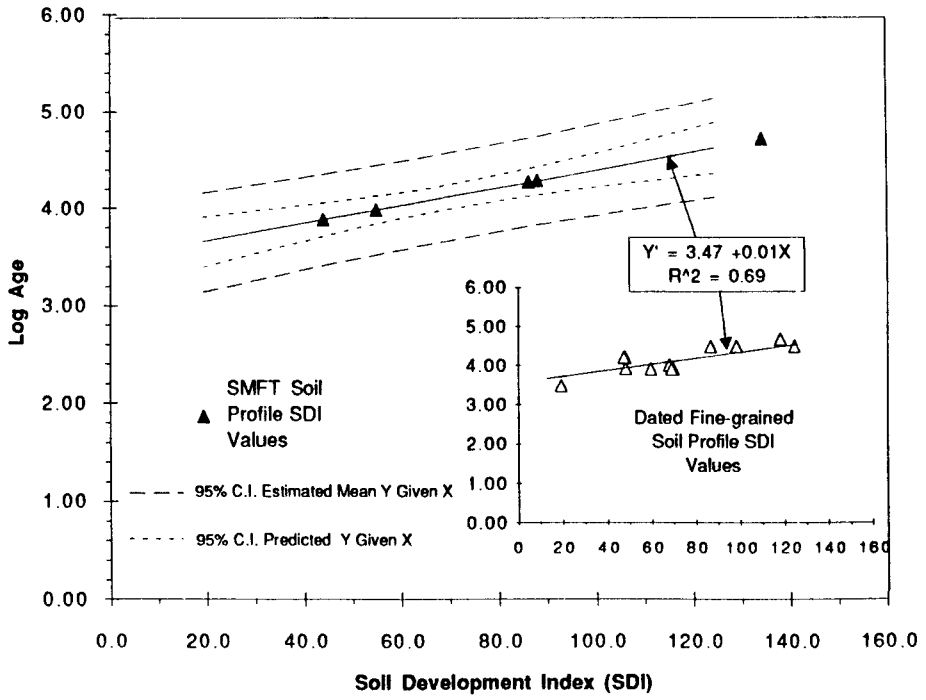

Figure A1. Soil development index (SDI) parameters for soil profiles in Santa Monica fault trenches. Soil profile locations as in Table A1. Regression method is from Rockwell et al. (1990).

geles basin, California: Geological Society of America Bulletin, v. 109, p. 1595–1616.

Dolan, J.F., Stevens, D., and Rockwell, T.K., 2000, Paleoseismologic evidence for an early to mid-Holocene age of the most recent surface rupture on the Hollywood fault, Los Angeles, California: Bulletin of the Seismological Society of America, v. 90, p. 330–344.

Drumm, P.L., 1992, Holocene displacement of the central splay of the Malibu Coast fault zone, Latigo Canyon, Malibu, *in* Pipkin, B., and Proctor, R., eds., Engineering geology practice in southern California: Belmont, California, Star Publishing Company, p. 247–254.

Ellsworth, W.L., 1990, Earthquake history, 1769–1989, *in* Wallace, R.E., ed., The San Andreas fault system, California: U.S. Geological Survey Professional Paper 1515, p. 153–187.

Hanks, T.C., Hileman, J.A., and Thatcher, W., 1975, Seismic moments of the larger earthquakes of the southern California region: Geological Society of America Bulletin, v. 86, p. 1131–1139.

Harris, R.A., and Day, S.M., 1993, Dynamics of fault interaction: Parallel strike-slip faults: Journal of Geophysical Research, v. 98, p. 4461–4472.

Harris, R.A., and Day, S.M., 1998, Dynamic 3D simulations of earthquakes on en echelon faults: Geophysical Research Letters, v. 26, p. 2089–2092.

Hauksson, E., 1990, Earthquakes, faulting, and stress in the Los Angeles basin: Journal of Geophysical Research, v. 95, p. 15365–15394.

Heaton, T.H., Hall, J.F., Wald, D.J., and Halling, M.W., 1995, Response of high-rise and base-isolated buildings to a hypothetical M_w 7.0 blind thrust earthquake: Science, v. 267, p. 206–211.

Hill, R.L., 1979, Potrero Canyon fault and University High School escarpment, *in* Field guide to selected engineering and geologic features, Santa Monica Mountains, *in* Keaton, J.R., ed., Chairman: Southern California Section, Association of Engineering Geologists, Annual Field Trip Guide, p. 83–103.

Hill, R.L., Sprotte, E.C., Bennett, J.H., Real, C.R., and Slade, R.C., 1979, Location and activity of the Santa Monica fault, Beverly Hills–Hollywood area, California, *in* Earthquake hazards associated with faults in the greater Los Angeles metropolitan area, Los Angeles County, including faults in the Santa Monica–Raymond, Verdugo–Eagle Rock, and Benedict Canyon fault zones: California Division of Mines and Geology Open-File Report 79–16 LA, p. B1–B43.

Hoots, H.W., 1931, Geology of the eastern part of the Santa Monica Mountains, Los Angeles County: U.S. Geological Survey Professional Paper 165-C, p. 83–134.

Johnson, H.R., 1932, Folio of plates to accompany geologic report for Quelinda Estate, Pacific Palisades: Unpublished Report.

Jones, L.M., Sieh, K.E., Hauksson, E., and Hutton, L.K., 1990, The 3 December 1988 Pasadena earthquake: Evidence for strike-slip motion on the Raymond fault: Seismological Society of America Bulletin, v. 80, p. 474–482.

Junger, A., and Wagner, H.C., 1977, Geology of the Santa Monica and San Pedro basins, California continental borderland: U.S. Geological Survey Miscellaneous Field Studies Map MF-820, scale 1:250 000.

Lajoie, K.R., Kern, J.P., Wehmiller, J.F., Kennedy, G.L., Mathieson, S.A., Sarna-Wojcicki, A.M., Yerkes, R.F., and McCrory, P.F., 1979, Quaternary marine shorelines and crustal deformation, San Diego to Santa Barbara, California, *in* Abbott, P.L., ed.: Geological Society of America Annual Meeting, Field Trip Guide, p. 3–15.

Liddicoat, J.C., 1992, Paleomagnetics of the Pico Formation, Santa Paula Creek, Ventura basin, California: Geophysical Journal International, v. 110, p. 267–275.

Liu, H., and Heaton, T., 1984, Ray analysis of ground velocities and accelerations from the 1971 San Fernando, California, earthquakes: Seismological Society of America Bulletin, v. 74, p. 1951–1968.

McGill, J.T., 1989, Geologic maps of the Pacific Palisades area, Los Angeles, California: U.S. Geological Survey Miscellaneous Investigations Series Map I-1828, scale 1:4800.

McNeilan, T., Rockwell, T.K., and Resnick, G., 1996, Sense and rate of Holocene slip, Palos Verdes fault, southern California: Journal of Geophysical Research, v. 101, no. B4, p. 8317–8334.

Muhs, D.R., Rockwell, T.K., and Kennedy, G.L., 1992, Late Quaternary uplift rates of marine terraces on the Pacific coast of North America, southern Oregon to Baja California Sur: Quaternary International, v. 7/8, p. 81–93.

Muhs, D.R., Kennedy, G.L., and Rockwell, T.K., 1994, Uranium-series ages of marine terrace corals from the Pacific coast of North America and implications for last-interglacial sea level history: Quaternary Research, v. 42, p. 72–87.

Olsen, K.B., and Archuleta, R.J., 1996, Site response in the Los Angeles basin from 3-D simulations of ground motion [abs.]: Seismological Research Letters, v. 67, p. 49.

Patterson, R.H., 1979, Tectonic geomorphology and neotectonics of the Santa Cruz Island fault, Santa Barbara County, California [M.S. thesis]: Santa Barbara, University of California, 140 p.

Pinter, N., and Sorlien, C., 1991, Evidence for latest Pleistocene to Holocene movement on the Santa Cruz Island fault, California: Geology, v. 19, p. 909–912.

Pinter, N., Lueddecke-Pinter, S., and Keller, E.A., 1995, Short-term and long-term activity on the Santa Cruz Island fault, California: Geological Society of America Abstracts with Programs, no. 6, v. 27, p. A-375.

Pratt, T.L., Dolan, J.F., Odum, J.K., Stephenson, W.J., Williams, R.A., and Templeton, M.E., 1998, Multi-scale seismic imaging of active fault zones for seismic hazard assessment: A case study of the Santa Monica fault zone, Los Angeles, California: Geophysics, v. 63, p. 479–489.

Rockwell, T.K., 1994, Rectifying disparate Stage 5 paleosea level estimates from California, New Guinea and Japan: Geological Society of America Abstracts With Programs, v. 26, no. 7, p. A-515.

Rockwell, T.K., Loughman, C., and Merifield, P., 1990, Late Quaternary rate of slip along the San Jacinto fault zone near Anza, southern California: Journal of Geophysical Research, v. 95, p. 8593–8605.

Rockwell, T.K., Muhs, D.R., and Kennedy, G.L., 1992, Late Quaternary paleo-sea level estimates for the west coast of North America based on coral-dated marine terraces, International Geological Correlation Programme 274 Symposium on Diversity in Coastal Evolution in the Quaternary, Programme and Abstracts, p. 47.

Schneider, C.L., Hummon, C., Yeats, R.S., and Huftile, G.L., 1996, Structural evolution of the northern Los Angeles basin, California, based on growth strata: Tectonics, v. 15, p. 341–355.

Scientists of USGS/SCEC, 1994, The magnitude 6.7 Northridge, California, earthquake of 17 January 1994: Science, v. 266, p. 389–397.

Shaw, J.H., and Shearer, P., 1999, An elusive blind-thrust fault beneath metropolitan Los Angeles: Science, v. 283, p. 1516–1518.

Shaw, J.H., and Suppe, J., 1994, Active faulting and growth folding in the eastern Santa Barbara Channel, California: Geological Society of America Bulletin, v. 106, p. 607–626.

Shaw, J.H., and Suppe, J., 1996, Earthquake hazards of active blind-thrust faults under the central Los Angeles basin, California: Journal of Geophysical Research, v. 101, p. 8623–8642.

	MHI	Log Age	95% C.I.		Age	Max	Min
SMFT 1a (Unit 2)	0.58	4.33	4.97	3.69	21,353	92,948	4,986
SMFT 1a (Unit 3)	0.56	4.28	4.94	3.61	19,813	87,918	4,112
SMFT 1b (Unit 2)	0.63	4.46	5.12	3.79	28,542	131,518	6,194
SMFT 1c (Unit 3)	0.61	4.41	5.08	3.73	25,414	119,708	5,395
SMFT 4a	0.71	4.66	5.33	3.99	45,486	211,956	9,727
SMFT 4b	0.58	4.13	4.83	3.43	13,422	66,923	2,692

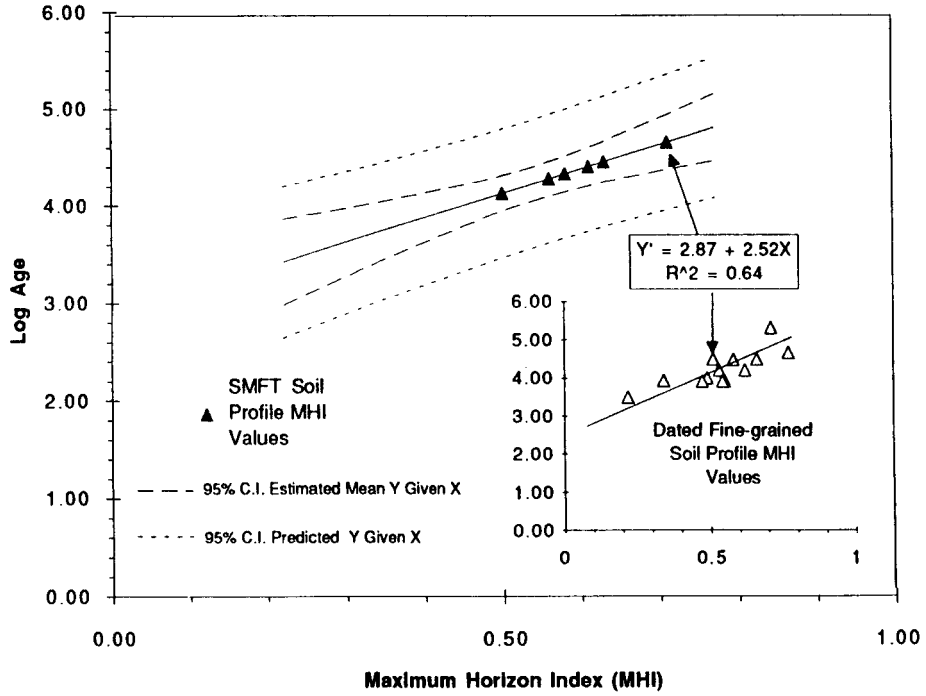

Figure A2. Maximum horizon index (MHI) parameters for soil profiles in Santa Monica fault trenches. Soil profile locations as in Table A1. Regression method is from Rockwell et al. (1990).

Sibson, R.H., 1985, Stopping of earthquake ruptures at dilational fault jogs: Science, v. 316, p. 248–251.

Sorlien, C.C., 1994, Faulting and uplift of the northern Channel Islands, California, *in* Halvorson, W.L., and Maender, G.J., eds., Proceedings, Fourth Channel Islands Symposium: Update on the status of resources: Santa Barbara, California, Santa Barbara County Museum of Natural History, p. 281–296.

Stein, R.S., and Thatcher, W., 1981, Seismic and aseismic deformation associated with the 1952 Kern County, California, earthquake and relationship to the Quaternary history of the White Wolf fault: Journal of Geophysical Research, v. 86, p. 4913–4928.

Stephenson, W.J., Rockwell, T.K., Odum, J.K., Shedlock, K.M., and Okaya, D.A., 1995, Seismic reflection and geomorphic characterization of the onshore Palos Verdes fault zone, Los Angeles, California: Seismological Society of America Bulletin, v. 85, p. 943–950.

Stierman, D.J., and Ellsworth, W.L., 1976, Aftershocks of the February 21, 1973 Point Mugu, California earthquake: Seismological Society of America Bulletin, v. 66, p. 1931–1952.

Stuiver, M., and Reimer, P.J., 1993, Extended ^{14}C data base and revises CALIB 3.0 ^{14}C age calibration program: Radiocarbon, v. 35, p. 215–230.

Toppozada, T.R., Real, C.R., and Parke, D.L., 1981, Preparation of isoseismal maps and summaries of reported effects for pre-1900 California earthquakes: Sacramento, California Division of Mines and Geology Open-File Report 81–11, 182 p.

Toppozada, T., 1988, Planning scenario for a major earthquake on the Newport-Inglewood fault zone: San Francisco, California Division of Mines and Geology Special Publication, 99, 197 p.

Treiman, J.A., 1994, The Malibu Coast fault: California Division of Mines and Geology fault evaluation report FER 229: San Francisco, California Division of Mines and Geology, 42 p.

Tsutsumi, H., Yeats, R.S., Hummon, C., Schneider, C.L., and Huftile, G.J., 2000, Active and late Cenozoic tectonics of the northern Los Angeles fold-and-thrust belt, California: Geological Society of America Bulletin (in press).

Vedder, J.G., Greene, H.G., Clarke, S.H., and Kennedy, M.P., 1986, Geologic map of mid-southern California continental margin (map 2A), *in* Greene, H., and Kennedy, M., eds., California continental margin geologic map series (area 2 of 7; map sheet 1 of 4): Menlo Park, California, U.S. Geological Survey, and Sacramento, California Division of Mines and Geology, scale 1:250 000.

Vidale, J.E., and Helmberger, D.V., 1988, Elastic finite-difference modeling of the 1971 San Fernando California earthquake: Seismological Society of America Bulletin, v. 78, p. 122–141.

Walls, C., Rockwell, T., Mueller, K., Bock, Y., Williams, S., Pfanner, J., Dolan, J., and Fang, P., 1998, Escape tectonics in the Los Angeles metropolitan region and implications for seismic risk: Nature, v. 394, p. 356–360.

Ward, S., and Valensise, G., 1994, The Palos Verdes terraces: Bathtub rings from a buried thrust fault: Journal of Geophysical Research, v. 99, p. 4485–4495.

Weaver, K.D., and Dolan, J.F., in press, Paleoseismology and seismic hazards of the Raymond fault, Los Angeles County, California: Bulletin of the Seismological Society of America, v. 90.

Weber, G.E., 1992, Determination of the initiation of slide movement, Big Rock Mesa landslide, Malibu, California, *in* Ehlig, P.L., and Steiner, E.A., eds., Engineering geology field trips: Orange County, Santa Monica Mountains, and Malibu, guidebook and volume: Berkeley, California, Association of Engineering Geologists, p. C-45–C-53.

Wehmiller, J.F., Lajoie, K.R., Kvenvolden, K.A., Peterson, E., Belknap, D.F., Kennedy, G.L., Addicott, W.O., Vedder, J.G., and Wright, R.W., 1977, Correlation and chronology of Pacific coast marine terrace deposits of continental United States by fossil amino-acid stereochemistry—Technique evaluation, relative ages, kinetic model ages, and geologic implications: U.S. Geological Survey Open-File Report 77–680, 191 p.

Wells, D., and Coppersmith, K., 1995, New empirical relationships among magnitude, rupture length, rupture width, rupture area, and surface displacement: Seismology Society of America Bulletin, v. 84, p. 974–1002.

Wesnousky, S., 1986, Earthquakes, Quaternary faults, and seismic hazard in California: Journal of Geophysical Research, v. 91, p. 12587–12631.

Working Group on California Earthquake Probabilities, 1995, Seismic hazards in southern California: Probable earthquakes, 1994 to 2024: Seismological Society of America Bulletin, v. 85, p. 379–439.

Wright, T.L., 1991, Structural geology and tectonic evolution of the Los Angeles Basin, *in* Biddle, K.T., ed., Active-margin basins: American Association of Petroleum Geologists Memoir 52, p. 35–106.

Ziony, J.I., and Jones, L.M., 1989, Map showing late Quaternary faults and 1978–84 seismicity of the Los Angeles region: U.S. Geological Survey Miscellaneous Field Studies Map MF-1964, scale 1:250 000.

MANUSCRIPT RECEIVED BY THE SOCIETY MARCH 11, 1998
REVISED MANUSCRIPT RECEIVED JULY 8, 1999
MANUSCRIPT ACCEPTED MARCH 14, 2000

Printed in the USA